AD NUMBER
AD489258
LIMITATION CHANGES
TO: **Approved for public release; distribution is unlimited.**
FROM: **Distribution authorized to U.S. Gov't. agencies and their contractors; Critical Technology; SEP 1966. Other requests shall be referred to Arnold Engineering Development Center, Arnold Air Force Station, TN. This document contains export-controlled technical data.**
AUTHORITY
AEDC ltr, 23 Jan 1975

AEDC-TR-66-162

ay 1

AERODYNAMIC FORCES ON THE SNAP-19 FUEL CAPSULE AND NIMBUS B SOLAR PANEL AT A SIMULATED HIGH ALTITUDE

David E. Boylan
ARO, Inc.

September 1966

VON KÁRMÁN GAS DYNAMICS FACILITY
ARNOLD ENGINEERING DEVELOPMENT CENTER
AIR FORCE SYSTEMS COMMAND
ARNOLD AIR FORCE STATION, TENNESSEE

NOTICES

AERODYNAMIC FORCES ON THE SNAP-19 FUEL CAPSULE AND NIMBUS B SOLAR PANEL AT A SIMULATED HIGH ALTITUDE

David E. Boylan
ARO, Inc.

FOREWORD

The work reported herein was done at the request of the Arnold Engineering Development Center (AEDC), Air Force Systems Command (AFSC) for the Atomic Energy Commission and the Martin Company under AEC SNAP-19 Program AEC Activity Number 04-60-50-01.1.

The results of tests presented were obtained by ARO, Inc. (a subsidiary of Sverdrup & Parcel and Associates, Inc.), contract operator of AEDC, AFSC, Arnold Air Force Station, Tennessee, under Contract AF 40(600)-1200. The test was conducted from May 31 to June 3, 1966, under ARO Project No. VT1682, and the manuscript was submitted for publication on July 28, 1966.

This technical report has been reviewed and is approved.

Donald E. Beitsch
Major, USAF
AF Representative, VKF
Directorate of Test

Leonard T. Glaser
Colonel, USAF
Director of Test

ABSTRACT

Aerodynamic forces on a SNAP-19 fuel capsule and Nimbus B solar panel model were determined over an angle-of-attack range from 0 to 90 deg at a simulated high altitude under hypersonic, cold-wall conditions. Very large viscous-induced effects on aerodynamic drag, lift, and pitching moment were observed. The configurations were unstable about their mid-chord positions except near zero lift. Comparisons are made with inviscid (Newtonian) and free-molecular flow predictions. Altitude simulated for the full-scale configurations was approximately 260, 000 ft for the fuel capsule and 300, 000 ft for the solar panel.

CONTENTS

ILLUSTRATIONS

TABLE

NOMENCLATURE

A	Moment arm
A_{ref}	Reference area
C_A	Axial-force coefficient
C_D	Drag coefficient
$(C_D)_T$	Tare drag coefficient
C_L	Lift coefficient
$(C_L)_T$	Tare lift coefficient
$(C_M)_{0.5\ell}$	Pitching-moment coefficient about the midchord point
$(C_M)_b$	Pitching-moment coefficient about the model base
C_N	Normal-force coefficient
C_∞	Chapman-Rubesin viscosity relation $(\mu_w/\mu_\infty)(T_\infty/T_w)$
D	Drag force
F	Restoring force on balance
L	Lift force
L_{ref}	Reference length used in moment calculations
M_p	Static pitching moment
M_∞	Free-stream Mach number
p_o	Total pressure

q_∞	Free-stream dynamic pressure
Re_∞	Free-stream Reynolds number
T_o	Total temperature
$\overline{V}_\infty$	Viscous interaction parameter $M_\infty (C_\infty / Re_{\infty, L})^{1/2}$
α	Angle of attack
λ_∞	Free-stream mean free path

SUBSCRIPTS

1, 2, 3	Moment arms on balance components
b	Model base
L	Model reference length used in similarity parameters (see Fig. 2)

SECTION I
INTRODUCTION

The experimental determination of the aerodynamic characteristics of vehicles of complex geometry in conditions simulating flight at extreme altitudes has become increasingly important. This is attributable, in part, to the complexity of the flow model required for an adequate theoretical analysis in the transitional flow regimes. Therefore, recourse to wind tunnels providing simulation of flight at high altitudes is necessary.

In the present study the aerodynamic forces on the SNAP-19 fuel capsule and a solar panel to be used on the Nimbus B satellite were determined at a simulated high altitude. The accurate determination of the aerodynamic and aerothermodynamic behavior of the fuel capsule as it re-enters the earth's atmosphere is necessary from safety considerations.

SECTION II
APPARATUS

2.1 WIND TUNNEL

The investigation was conducted in the low density hypervelocity tunnel (Gas Dynamic Wind Tunnel, Hypersonic (L)) of the von Kármán Gas Dynamics Facility (VKF), AEDC. This tunnel is a continuous-type arc-heated, ejector-pumped facility, normally using nitrogen or argon as the test gas. A general description is contained in Appendix I.

2.2 AERODYNAMIC NOZZLE

The nozzle used for the present investigation is an axisymmetric, contoured nozzle with no flow gradients in the test section. The useful test core has approximately 1.5-in. diameter and 8.0-in. length. Flow conditions for this nozzle are listed in the following table.

Gas	Nitrogen
p_o, $lb_f/in.^2$	25
T_o, °K	1660
M_∞	9.37
Re_∞, $in.^{-1}$	1600
q_∞, psf	8.25
λ_∞, in.	0.0086*

*For a static gas of billiard-ball molecules.

Diagnostic techniques for flow calibration are mentioned in Appendix I

2.3 TEST MODELS

Test configurations consisted of three 12.27-percent scale models of the SNAP-19 fuel capsule and five 0.668-percent scale models of the solar panel. Figure 1 is a photograph of the test configurations, and Fig. 2 indicates pertinent model dimensions, reference areas, lengths, and angle-of-attack range investigated with each model. A series of small sting adapters constructed to give 5-deg increments in angle of attack allowed α to be varied from 0 to 90 deg. Simulation of the solar panel thickness was not possible because of the extremely thin model which would be required (0.0038 in.). For this reason two thicknesses were tested to obtain information on the effect of this approximation of model scaling.

2.4 THREE-COMPONENT FORCE BALANCE

The balance is of the external type and is composed of two lift and two drag components, with pitching moment being derived from these components. Although the two drag components could be used to determine yawing moment, only pitching moment is measured at this time. All components are operated on the nulling principle. Figure 3 indicates the mechanical arrangement of the balance, and Ref. 1 gives a complete description, with a discussion of the balance performance evaluation and accuracy.

The aerodynamic pitching moment of the model is resolved from the lift and drag forces and measured moment-arm lengths. The following sketch illustrates the method by which the pitching moment is determined.

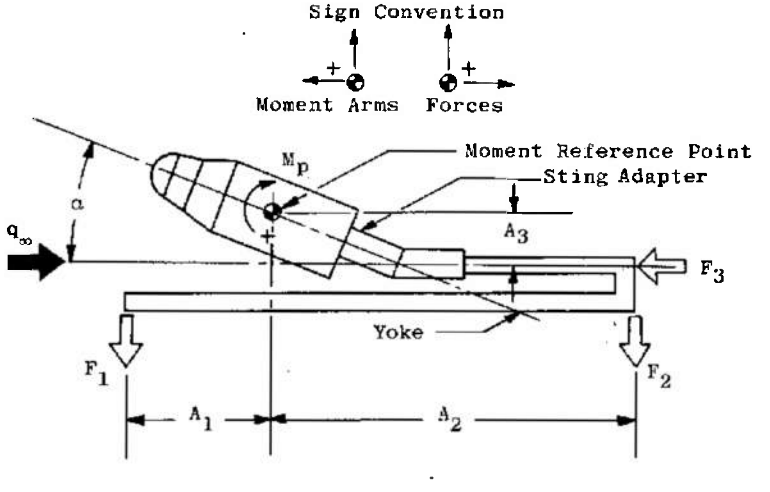

From the sketch it can be seen that the sum of all moments about the moment reference point is $M_p + F_1A_1 + F_2A_2 + F_3A_3 = 0$ where F_1, F_2, and F_3 are balance restoring or reaction forces of appropriate sign.

The distances A_1 and A_2 are determined from the known distance between components F_1 and F_2 and the measured position of the model moment reference point. Length A_3 is determined by the positions of the sting centerline and the moment reference point of the body.

The lift and drag aerodynamic loads experienced during the tests were of a magnitude that would, except for the lift components near zero angle of attack, be well within the accuracy limit of the balance. For comparative purposes and error estimates, the following values may be used.

	Maximum Load, lb_f or in.-lb_f	Accuracy, lb_f or in.-lb_f
Drag	2.6×10^{-2}	2×10^{-4}
Lift	$+6.5 \times 10^{-3}$ -1.0×10^{-3}	$\pm 4 \times 10^{-5}$

A discussion of the pitching moments is given in a later section.

SECTION III
EXPERIMENTAL PROCEDURES AND RESULTS

Tunnel L is capable of continuous operation for several hours if desired. However, force test runs are normally limited to approximately 30 sec to prevent excessive heating of the balance and models and to maintain cold-wall ($T_w << T_o$) conditions. The data have been reduced to coefficient form using reference areas and lengths as defined in Fig. 2. Testing at each angle of attack was repeated several times. The data repeated within ±5 percent, and data listed herein represent averages of these several runs. Table I contains values of C_L, C_D, and, where applicable, $(C_M)_{0.5\ell}$ and $(C_M)_b$. Also listed are values of C_N and C_A, as converted from measured lift and drag forces.

Previous measurements, at the flow conditions of the present test, using internal thermocouples installed on thin-walled, blunt models indicated that the wall-to-stagnation temperature ratio is in the range

$0.3 \leq T_w/T_o \leq 0.5$ with the higher value existing only near the stagnation point. A value of $T_w/T_o \approx 0.3$ is estimated to represent the average wall temperature over a large portion of the model surface.

The altitude simulation for each model, based on various simulation parameters, is tabulated in the following table.

Model	Simulated Altitude, ft x 10^{-3}		
	$Re_{\infty, L}$	$\bar{V}_{\infty, L}$	Kn_L
Fuel Capsule	277	247	245
Solar Panel	320	277	295

Calculations are based on full-scale lengths of 6.11 and 96 in. and velocities of 24,000 and 25,000 fps for the fuel capsule and solar panel, respectively. The standard atmosphere of Ref. 2 was assumed.

3.1 FUEL CAPSULE

Figure 4 shows C_L, C_D, C_M, C_N, and C_A as functions of angle of attack over the range $0 \leq \alpha \leq 90$ deg for the fuel capsule configuration. The data have been adjusted for a slight sting deflection. This correction was accomplished by obtaining forces at negative as well as positive angles of attack and forcing symmetry of the data. The correction to α was less than 2 deg for all models. Data obtained at negative angles of attack have been plotted as positive, with appropriate sign changes, to obtain better definition of the data trends.

Figure 4a indicates lift coefficient, C_L, and absolute lift force, L, as measured by the balance. Also shown are available theoretical estimates for the two limits of inviscid Newtonian and free-molecular flow theory.

The inviscid-fluid force on a right circular cylinder, neglecting the effect of the front force, is given by (Ref. 3), viz,

$$C_N = 3.479 \sin^2 \alpha \qquad C_A = 0 \qquad (1)$$

with the reference area taken as the cross-sectional area, a length-to-diameter ratio of 2.05, and Newtonian impact constant, K, assumed to be 2.0. For the front face (disk),

$$C_N = 0$$
$$C_A = 2 \cos^2 \alpha \qquad (2)$$

Combining Eqs. (1) and (2), the Newtonian predictions of C_N, C_A, C_L, and C_D were calculated for the complete configuration. Static pitching moment taken about the mid-chord point is zero in this context.

The determination of aerodynamic forces acting on bodies in a free-molecular flow is of interest in satellite design and to establish very useful limits to data such as are presented herein. One of the more recent studies for the prediction of these forces is that of Ref. 4. The force on an element of area in free-molecular flow is derived with the following assumptions:

a. The surface is convex.

b. Completely diffused reflection exists.

c. The re-emitted molecules have a constant temperature for the entire surface area.

The analysis results in closed-form integral solutions for the aerodynamic forces on flat plates and cylindrical segments at arbitrary angles of attack. Actual configurations must be approximated by using these composite parts. Figure 4 shows the free-molecular-flow force coefficients for the test configuration computed by this technique for a free-stream molecular speed ratio of 8.0 assuming a reflected-to-incident temperature ratio of 5.2. These values approximate the flow conditions of the present test. Theoretical predictions neglect the small concave indentation at the front of the fuel capsule model and the finite solar panel model thickness.

A comparison of the data in Fig. 4a with Newtonian and free-molecular predictions indicates a reasonable trend for the altitude simulated in the present case. An interesting point is the increase in C_L near zero angle of attack. Data obtained on more conventional aerodynamic configurations at simulated high altitudes (Ref. 5) sometimes indicate a reduction in lift coefficient, C_L, as viscous effects increase. The effects of boundary-layer growth on the cylindrical portion of the configuration probably offset the large negative local component of lift induced by the flat front face.

Figure 4b indicates drag coefficient, C_D, and absolute drag force, D, as measured by the balance. Comparison with theoretical predictions again indicates a reasonable order of magnitude and data trend.

Static pitching moment is indicated in Fig. 4c. The moment reference point was taken at the 50-percent chord station on the model centerline. The moment is resolved from measured lift and drag forces as described in Section 2.4. The present conditions resulted in pitching moment, M_p, being between the limits $-7.0 \times 10^{-5} \lessapprox M_p \lessapprox 6.1 \times 10^{-4}$ in.-lb$_f$. This is approaching the accuracy of the balance which is considered to be $\pm 4 \times 10^{-5}$ in.-lb$_f$. In order to successfully resolve these data, it was necessary to use measurements with the model inverted, i.e., negative angle of attack, and correct each component of force individually for the small sting deflection which was present. These adjusted data were then plotted as a function of nominal angle of attack, and values read from the faired curves at increments of 5 deg. A plot of C_M versus C_L indicates a highly unstable characteristic for center of gravity at the mid-chord position, with an approach to neutral stability at zero lift, i.e., $\alpha = 0$ and 90 deg. Both Newtonian and free-molecular theories predict essentially zero moment about the mid-chord station. In order to obtain better resolution of the moment data, the lift and drag measurements were converted to values of C_N and C_A (Figs. 4d and e). Faired curves through the normal-force and pitching-moment data were then used to transfer the moment reference to the model base. The resulting moment curve is shown in Fig. 4f compared to Newtonian and free-molecular flow predictions. This procedure does not indicate the accuracy of the moment data since the transferred result is dependent on C_N, which is of considerably greater magnitude than $\left(C_M\right)_{0.5\ell}$. However, the resulting reasonable magnitude and trend suggested the advisability of using the base as the reference point. This procedure was followed and the results are shown in Fig. 4f. The close agreement between the values of $\left(C_M\right)_b$ and the transferred moment curve support the data shown in Fig. 4c. The large increase in normal force (Fig. 4d) induced by the high viscous stresses appears to cause the configuration to be highly unstable for center of gravity at the mid-chord position. These results contradict the inviscid and free-molecular flow predictions, showing the danger sometimes attending interpolations between those theoretical limits.

3.2 SOLAR PANEL

In order to mount the solar panel model on the force balance, a balance adapter as shown in Fig. 2b was necessary. It was recognized that considerable tare force would exist on models D and E because of this mounting arrangement when $0 \lessapprox \alpha \lessapprox 40$ deg. A dummy model, which was independently supported and could be pivoted to the correct angle of attack, was constructed, and tare force on the balance mounting adapter and sting adapter were measured. The results are shown in Fig. 5, referenced to the same area as that used for the solar panel models. Subsequent results shown for models D and E have been adjusted for these tare forces. Of course, this procedure yielded only the force on the balance and sting adapters in the presence of the model; it did not reveal the presumably finite interference force on the model.

Figure 6 shows the calculated free-molecular flow force coefficients for a free-stream molecular speed ratio of 8.0 assuming a reflected-to-incident temperature ratio of 5.2. Figure 6a indicates lift force coefficient, C_L, and absolute lift force, L, as measured by the balance. A small leading-edge thickness influence can be observed as well as a distinct shift in the data between the adjusted models D and E results and the remainder of the data. The indication is that the lift tare measurement did not fully account for the influence of the balance mounting adapter. Although a reasonably correct flow field was probably simulated in the tare force measurements, the upstream influence of the mounting adapter exerted on the solar panel was not measured. In addition, a considerable area of the plate was shielded inside the mounting adapter. Tare forces on models F, G, and H are considered to be essentially zero since the mounting adapter and sting adapters were hidden from the flow. Theoretical predictions, based on inviscid Newtonian and free-molecular flow, are compared to the measured results. Fortunately, in the region where doubt exists as to the accuracy of the data ($0 \lessapprox \alpha \lessapprox 30$ deg) the difference between the two theoretical limits is small.

The Newtonian predictions follow from Ref. 6 and are given by

$$C_L = 2 \sin^2 \alpha \cos \alpha \tag{3}$$

and

$$C_D = 2 \sin^3 \alpha \tag{4}$$

referenced to the planform area and assuming a Newtonian impact constant, K, of 2.0. Free-molecular flow calculations were performed as outlined in Section 3.1. Both predictions neglect the effect of leading-edge thickness; thus they are applicable more nearly to the full-scale configuration than the models used in the present investigation.

Figure 6b indicates drag coefficient, C_D, and absolute drag force, D, as measured by the balance. The correction for tare drag force appears to be much more satisfactory than was the case for the lift results. The effect of increasing the model leading-edge thickness appears to be negligible, although the finite leading-edge thickness does appear to increase the drag near zero angle of attack. This would indicate that the full-scale solar panel was not precisely scaled in the present investigation. A point of interest is the fact that the present experimental results approach Newtonian predictions as angle of attack approaches 90 deg. This would be expected because the relative drag component attributable to viscous stresses becomes progressively smaller on a flat plate as angle of attack is increased.

An attempt to obtain values of static pitching-moment coefficient, C_M, taken about the mid-chord position encountered the same difficulties as were discussed in regard to the fuel capsule model. In addition, the large tare forces which existed on model D resulted in unreliable pitching-moment data when referenced to the mid-chord position. The data were therefore reduced using the base of the model as the reference position. Small errors in individual drag component measurements are thereby suppressed because of the resulting large pitching moment. The results are shown in Fig. 6c compared to Newtonian and free-molecular flow predictions. Except near 90 deg angle of attack, the data trend and magnitude appear reasonable. Although Model H had the same thickness as the other models in Fig. 6c, it was hastily constructed during the course of the tests, and accurate determination of the required moment arms was not accomplished.

The lift and drag measurements were converted to normal- and axial-force coefficients and are shown in Figs. 6d and e. A smooth curve through the data of Fig. 6d (which exhibit tare force errors for $\alpha \lesssim 30$ deg) and Fig. 6c was then used to transfer the static pitching moment to the mid-chord position. The resulting moment curve is similar to the result for the fuel capsule configuration. However, precise definition of the magnitude is not possible because the terms $C_N/2$ and $(C_M)_b$ are almost equal, and their accuracy is not of the order which would be required for such a data adjustment. The data suggest that the solar panel is also highly unstable about the mid-chord position except near zero lift.

SECTION IV
CONCLUDING DISCUSSION

The results presented herein indicate that inviscid-fluid calculations of the aerodynamic forces on the SNAP-19 fuel capsule and Nimbus B solar panel are inadequate for the higher altitudes of atmospheric entry. Further, it is not always safe to interpolate between inviscid and free-molecule theoretical limits.

The static stability results indicate that both fuel capsule and solar panel are unstable relative to the 50-percent length station at the flow conditions of the present test. Both lift and drag coefficients reveal strong influences of the rarefied nature of the flow at the high altitude simulated in Tunnel L. Because of the small forces and relatively large tare corrections connected with the solar panel, those results must be treated with caution.

Other wind tunnel tests which are scheduled to be performed at $M_\infty \approx 10$ and Reynolds numbers corresponding to near-inviscid flow should be helpful in further understanding the aerodynamic behavior of these bodies. However, the importance of the wall-to-total temperature and wall-to-free-stream temperature ratios should be kept in mind when any such comparisons of data are attempted.

REFERENCES

1. Arney, G. D. and Harter, Wade T. "A Low-Load Three-Component Force Balance for Measurements in a Low-Density Wind Tunnel." AEDC-TDR-64-280 (AD453130), December 1964.

2. Minzner, R. A., Champion, K. S. W., and Pond, H. L. The ARDC Model Atmosphere, 1959, AFCRC-TR-59-267.

3. Clark, E. L. and Trimmer, L. L. "Equations and Charts for the Evaluation of the Hypersonic Aerodynamic Characteristics of Lifting Configurations by the Newtonian Theory." AEDC-TDR-64-25, March 1964.

4. Sentman, Lee H. "Free Molecule Flow Theory and its Application to the Determination of Aerodynamic Forces." LMSC-448814, October 1961.

5. Boylan, David E. and Potter, J. Leith. "Aerodynamics of Typical Lifting Bodies Under Conditions Simulating Very High Altitudes." AIAA Preprint 66-467, June 1966.

6. Hoerner, Sighard F. Fluid Dynamic Drag, Published by the author, 1958.

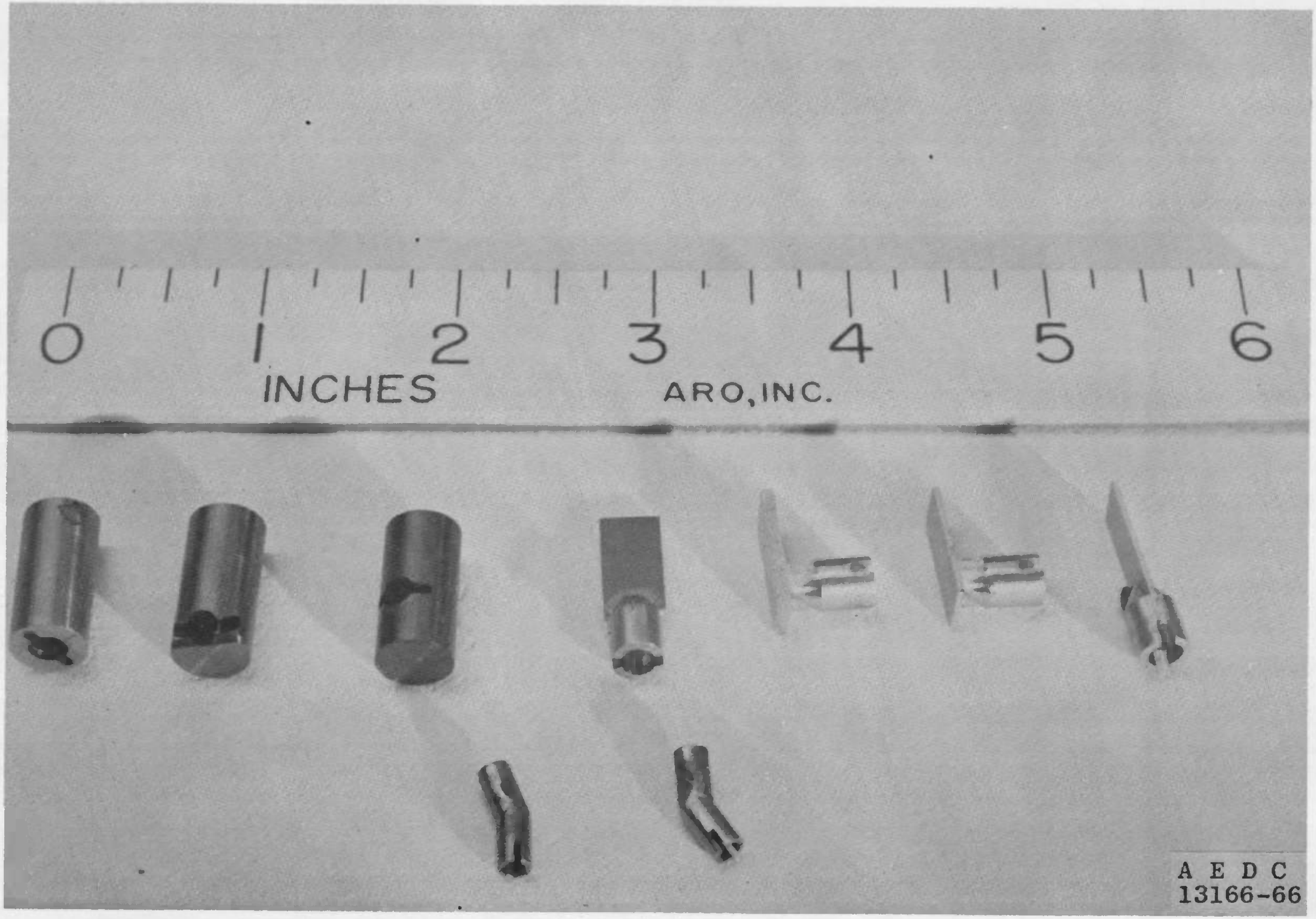

a. Photograph of Test Models

Fig. 1 Test Models

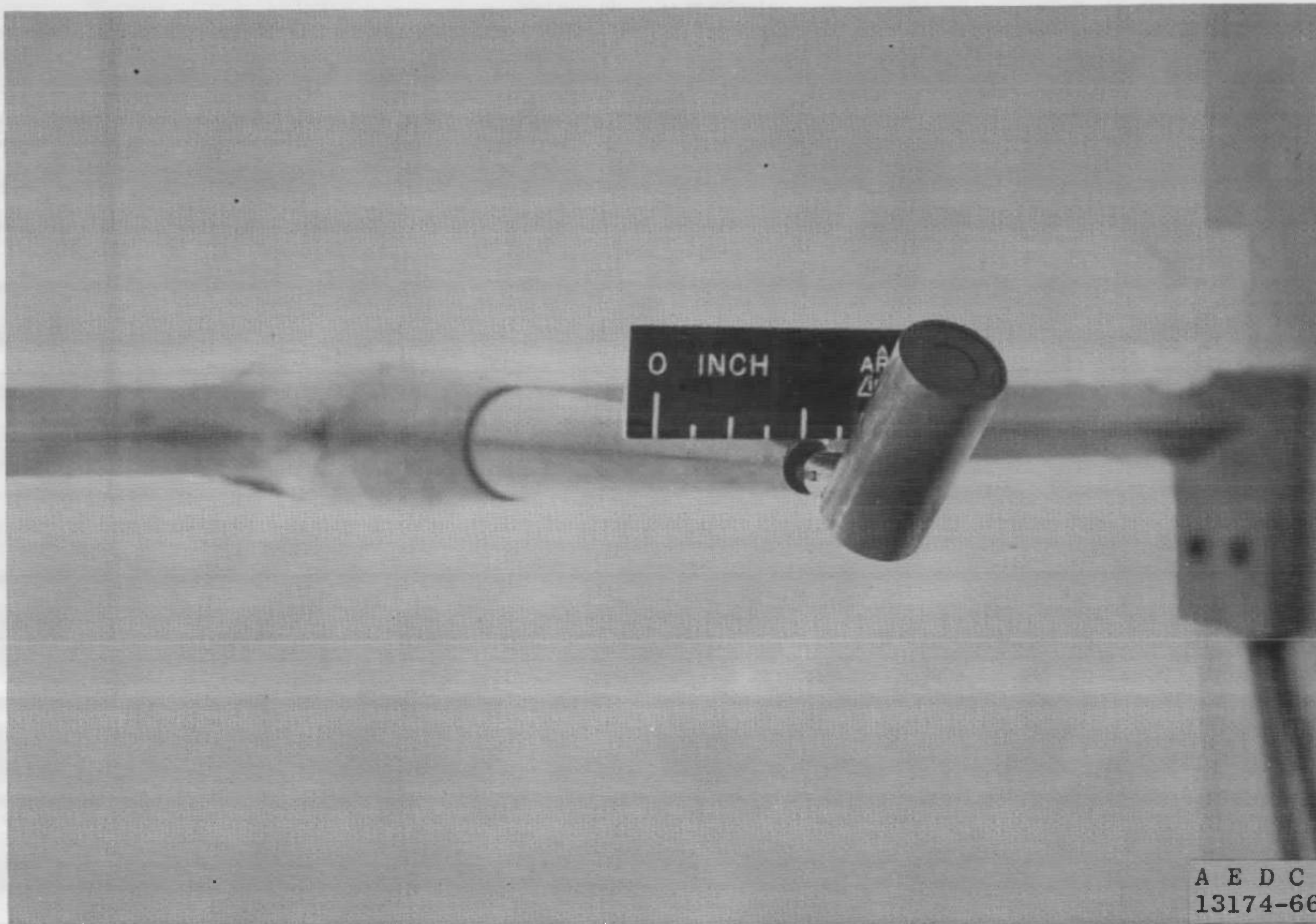

b. Model B Installed on Balance

Fig. 1 Concluded

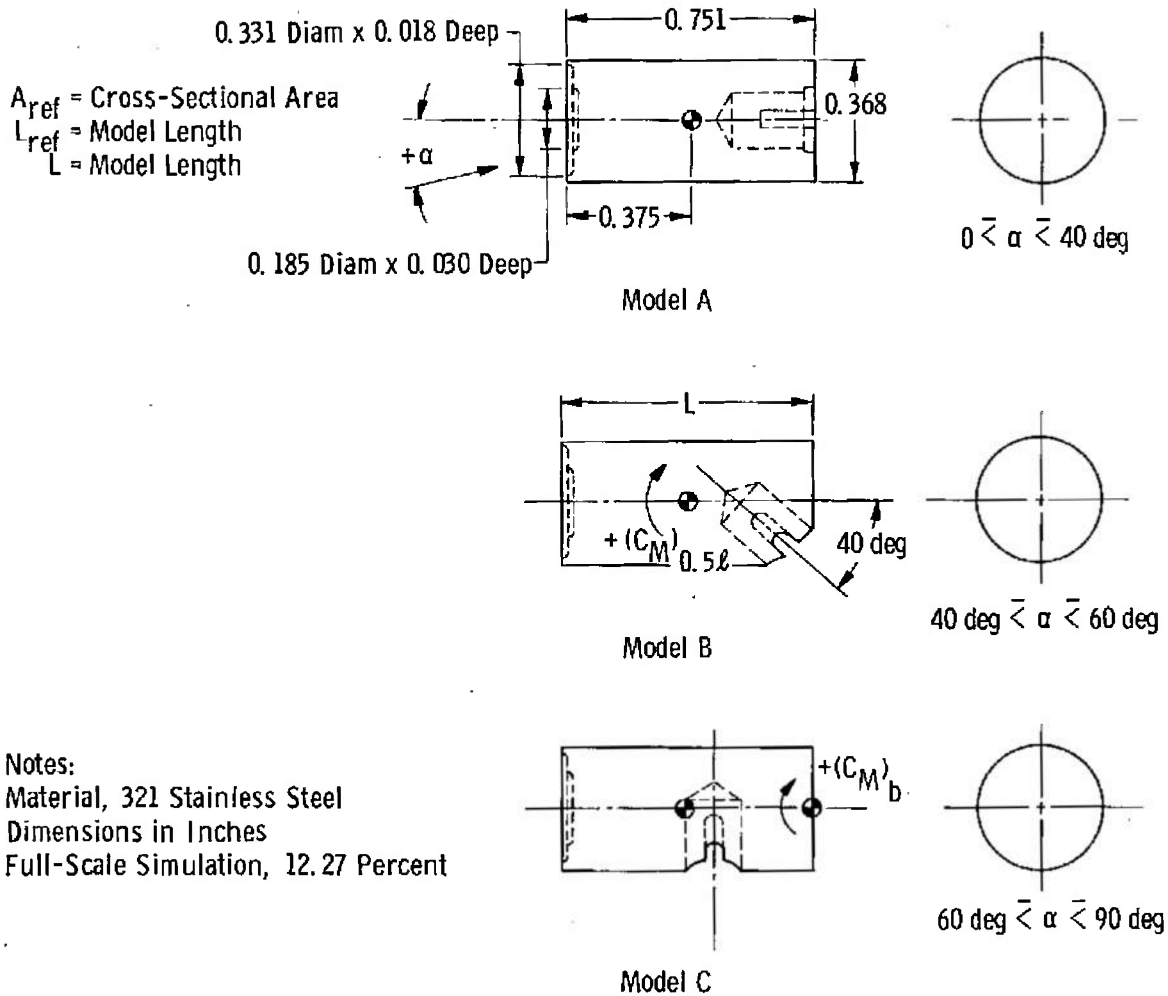

a. Fuel Capsule

Fig. 2 Model Dimensions

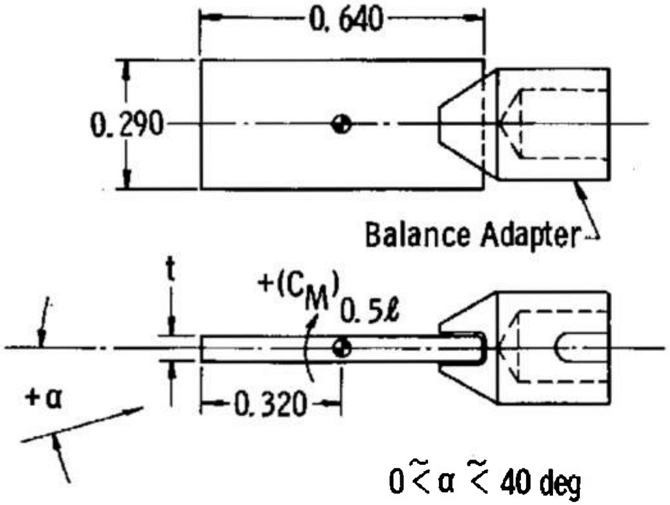

Models D and E

Model	t, in.
D	0.0315
E	0.0625
F	0.0315
G	0.0625
H	0.0315

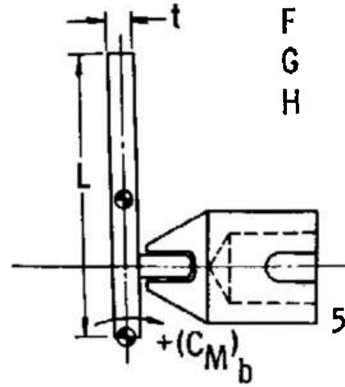

Models F and G

Notes:

A_{ref} = Planform Area

$L = L_{ref}$ = Model Length

Material, 303 Stainless Steel

Dimensions in Inches

Full-Scale Simulation, 0.668 Percent

Excluding Plate Thickness

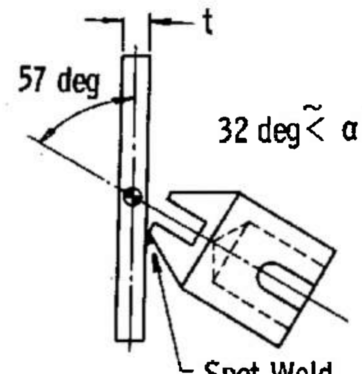

Model H

b. Solar Panel

Fig. 2 Concluded

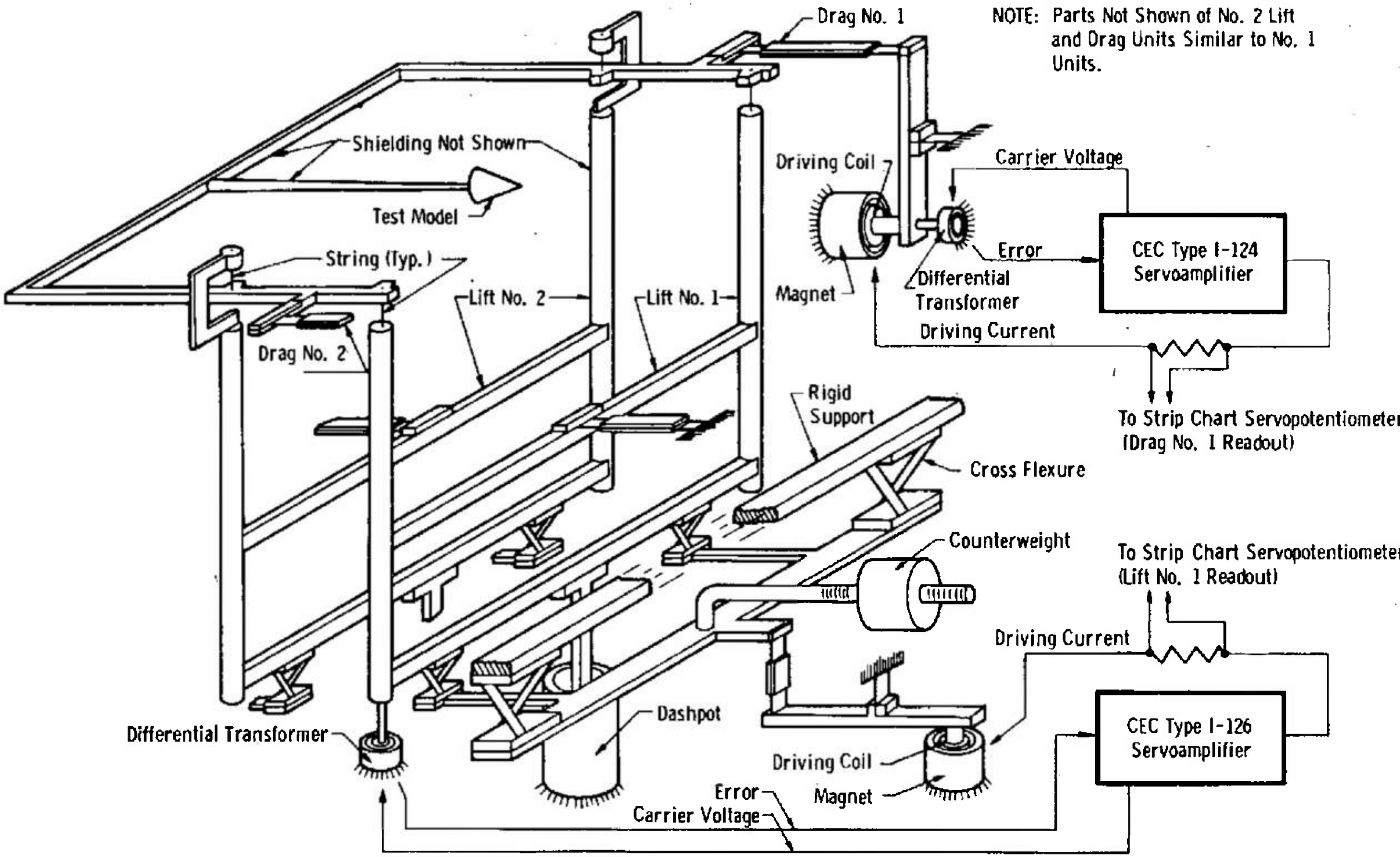

Fig. 3 Mechanical Arrangement of Balance

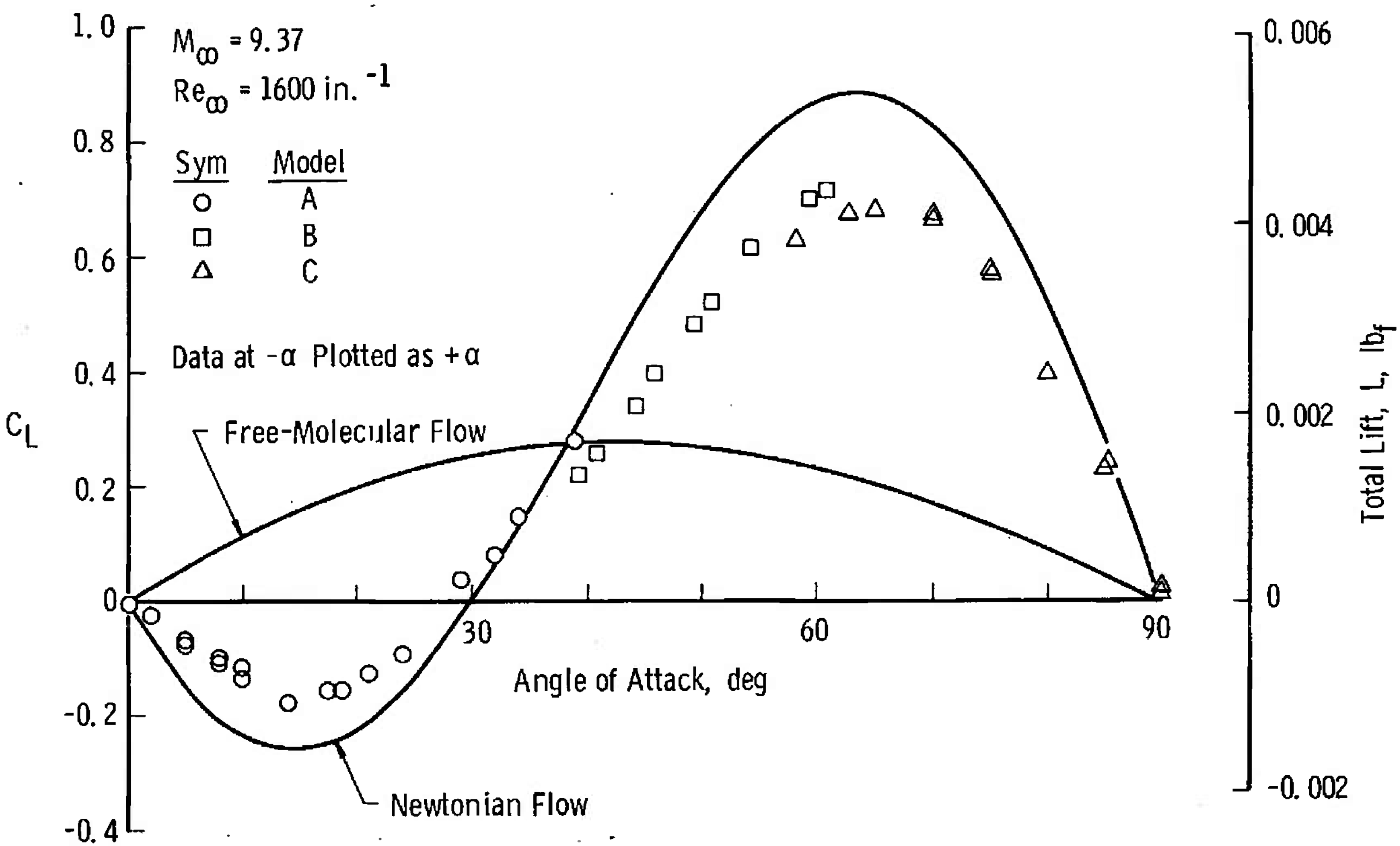

a. C_L as a Function of Angle of Attack

Fig. 4 Fuel Capsule Aerodynamic Forces

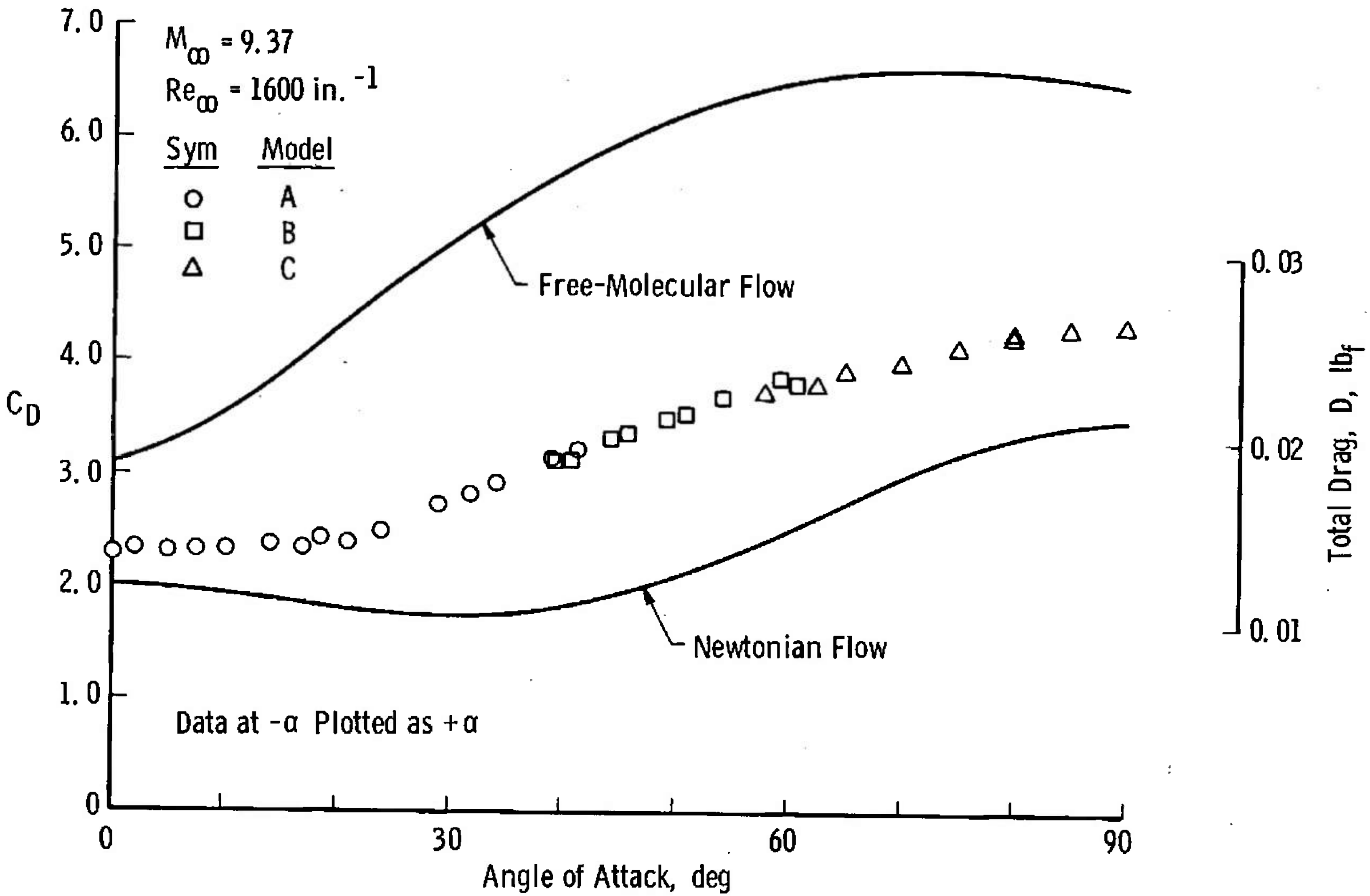

b. C_D as a Function of Angle of Attack

Fig. 4 Continued

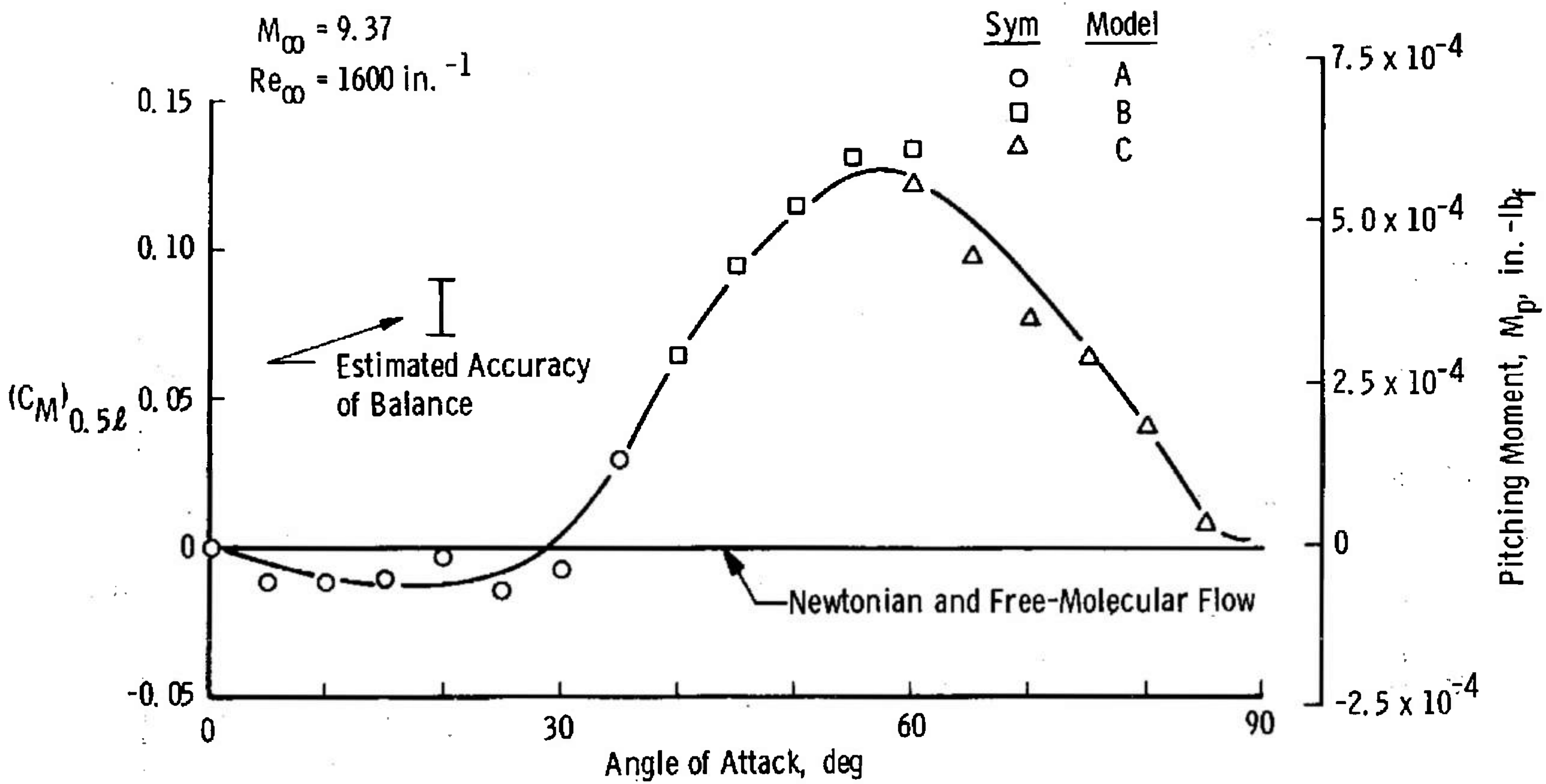

c. $(C_M)_{0.5\ell}$ as a Function of Angle of Attack

Fig. 4 Continued

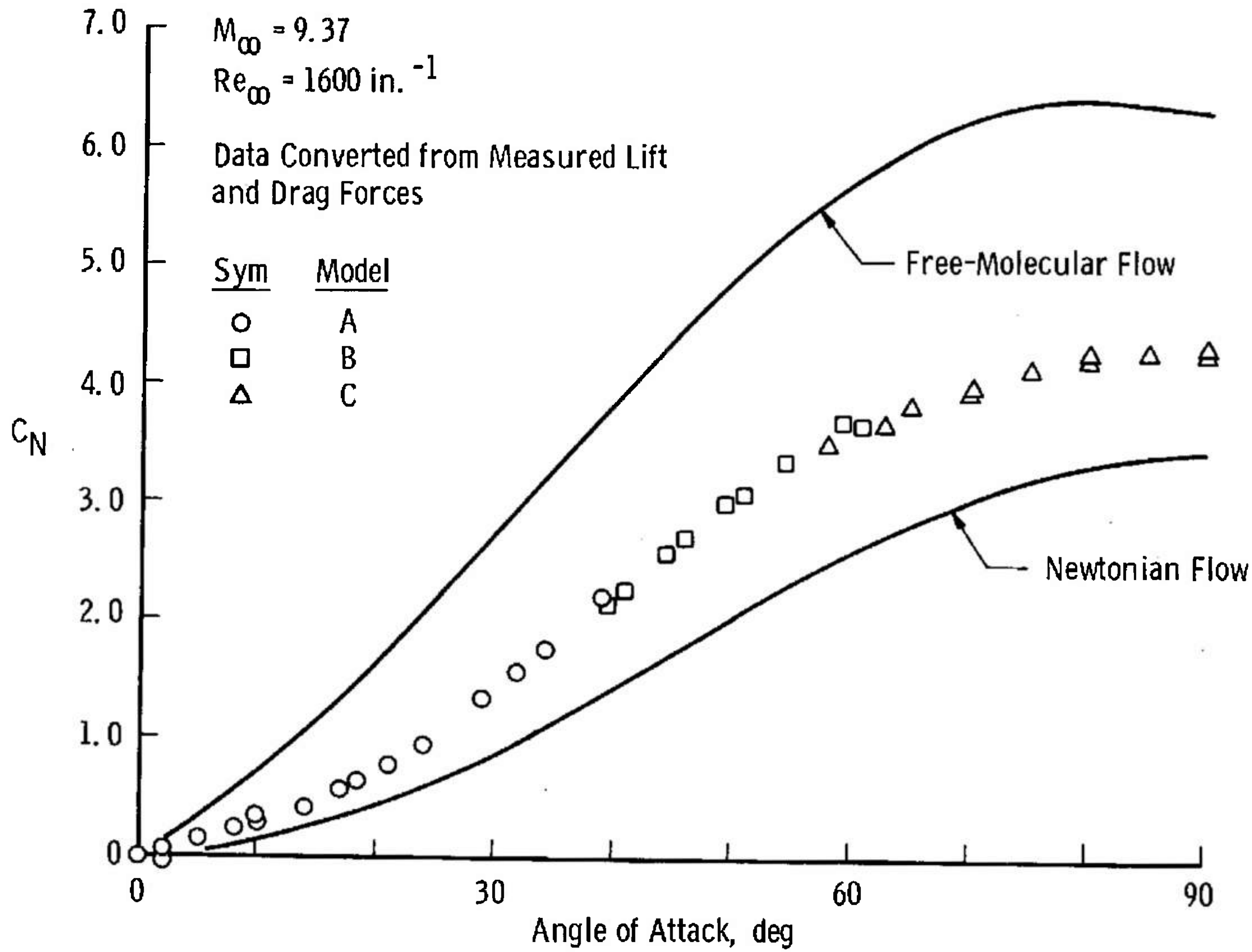

d. C_N as a Function of Angle of Attack

Fig. 4 Continued

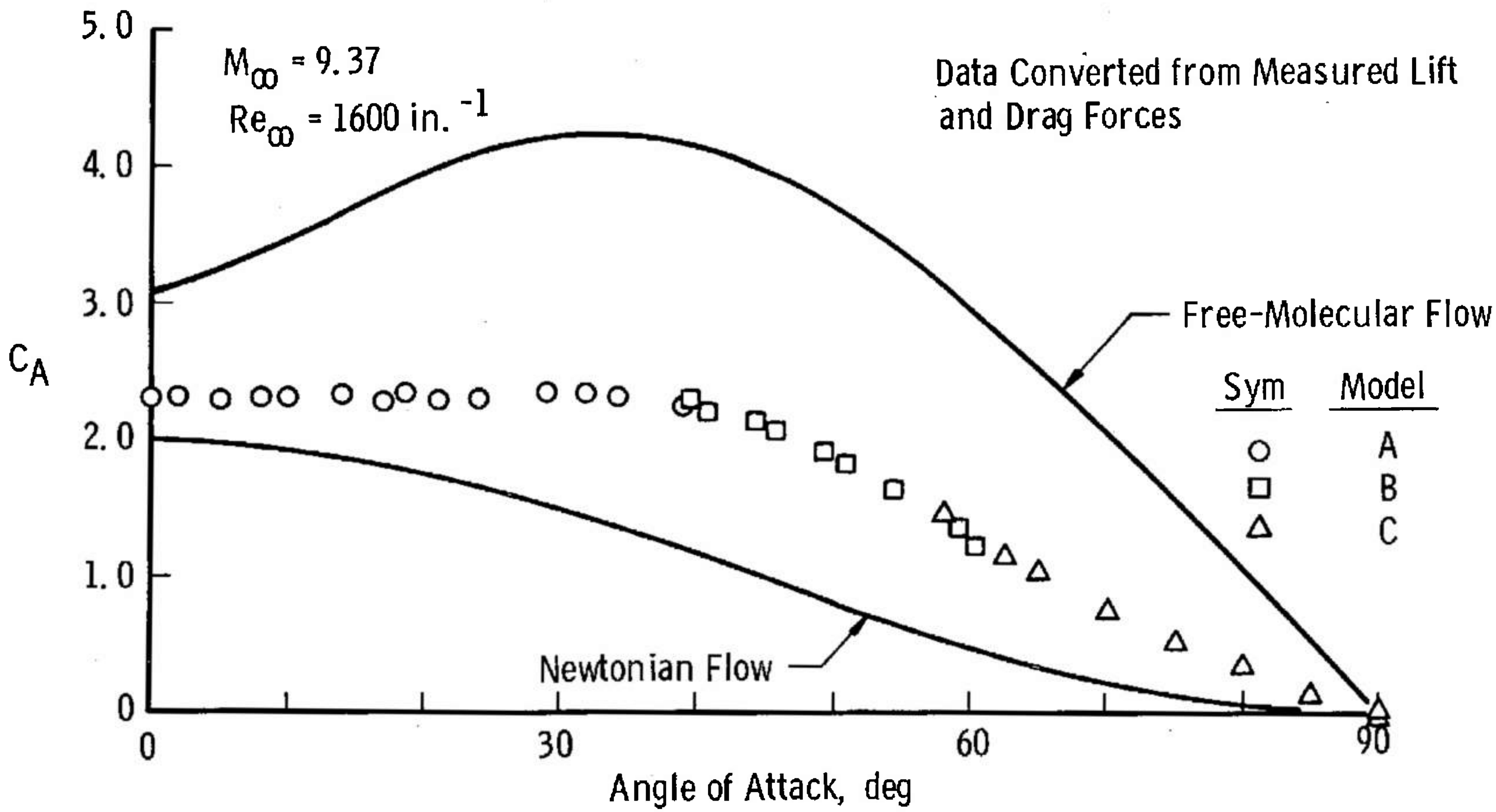

e. C_A as a Function of Angle of Attack

Fig. 4 Continued

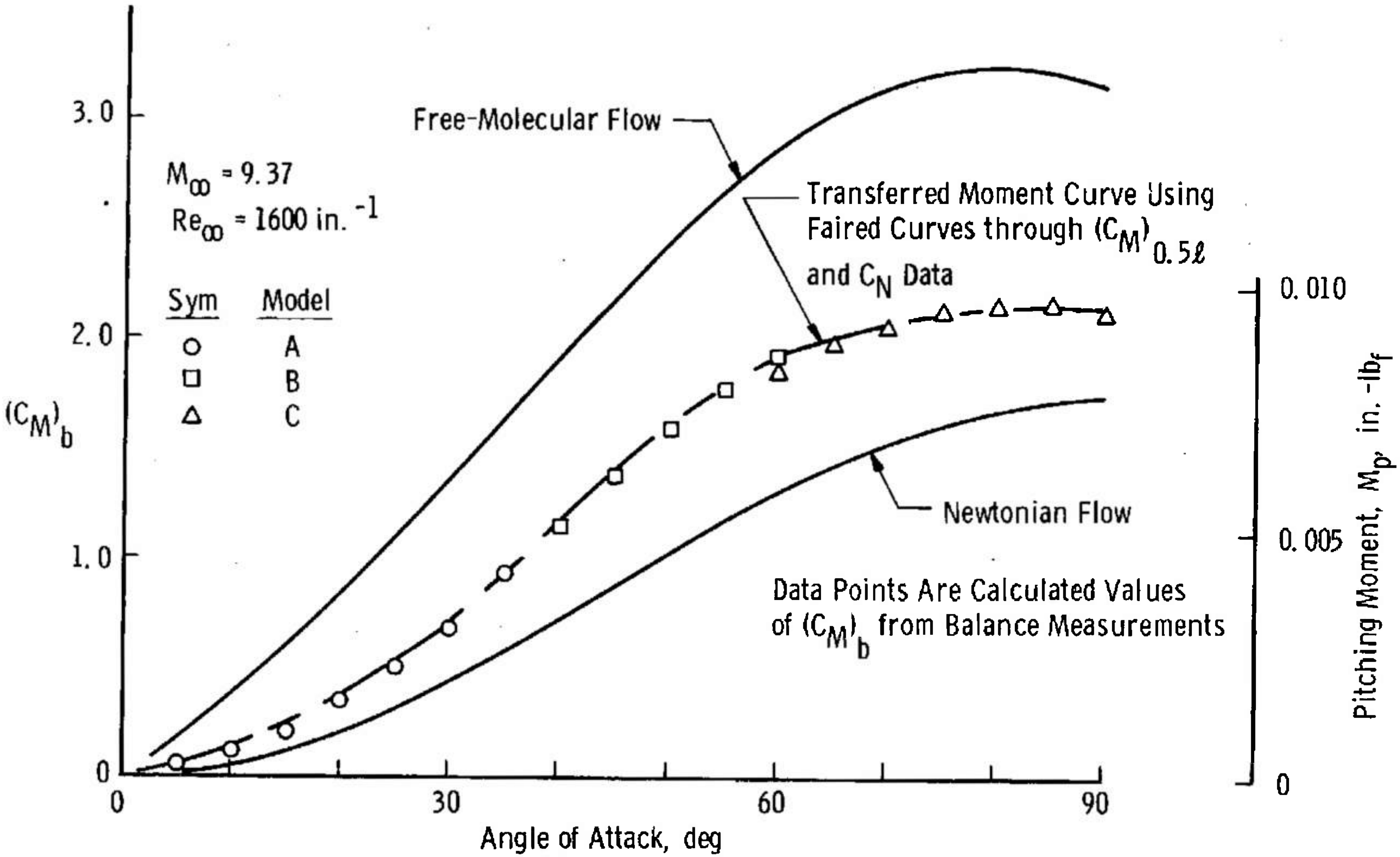

f. $(C_M)_b$ as a Function of Angle of Attack

Fig. 4 Concluded

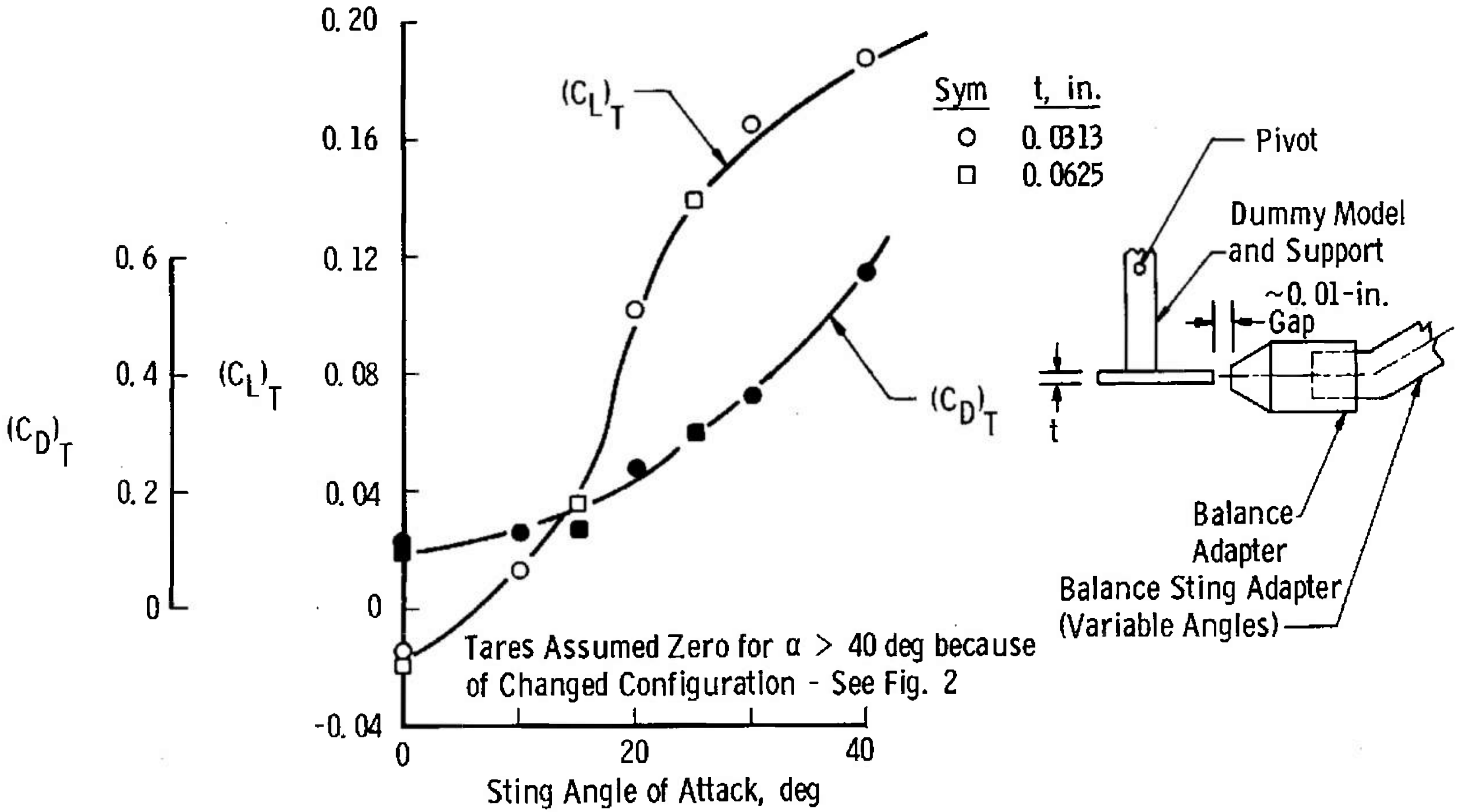

Fig. 5 Tare Force Measurement for Models D and E

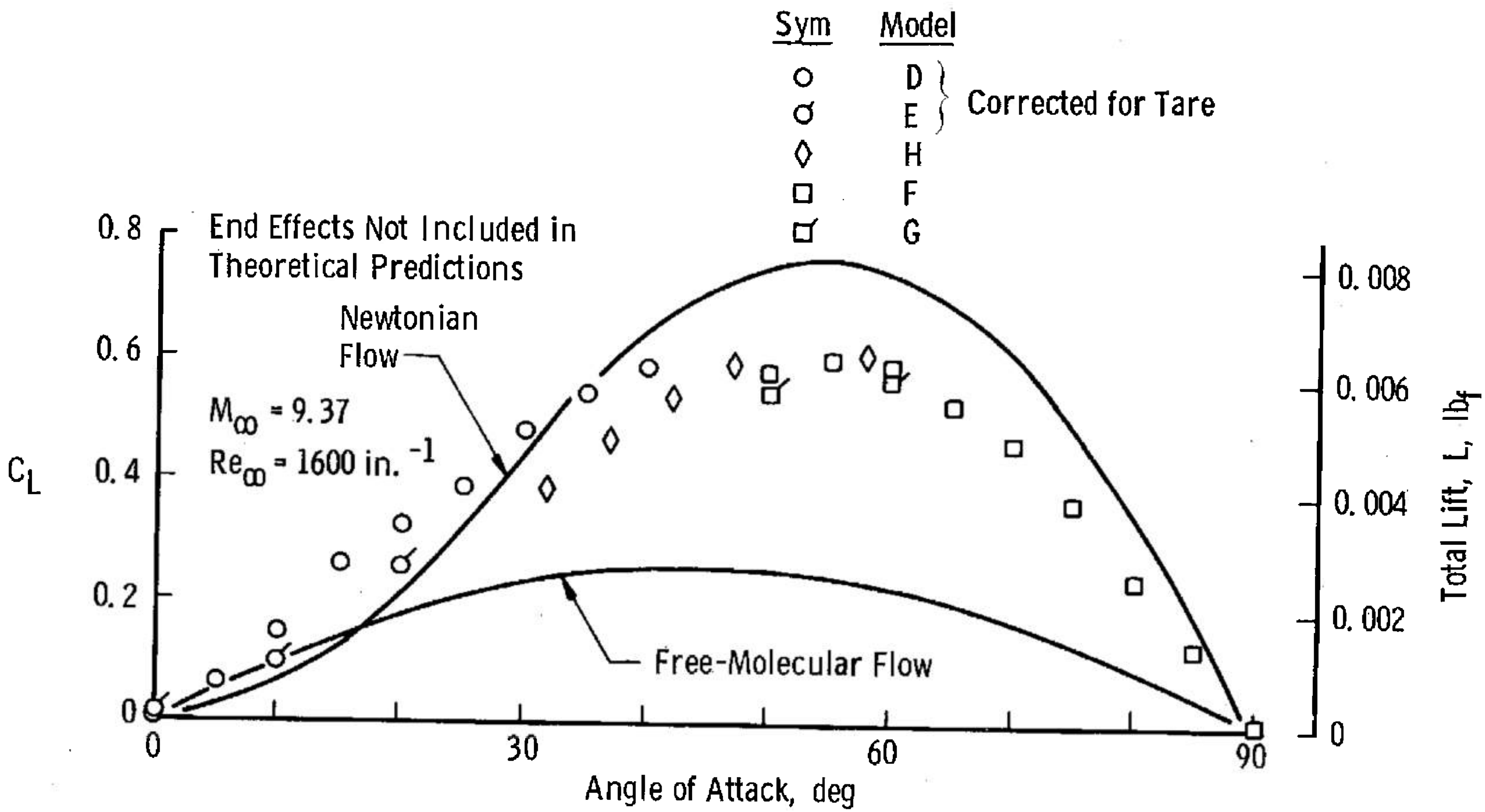

a. C_L as a Function of Angle of Attack

Fig. 6 Solar Panel Aerodynamic Coefficients

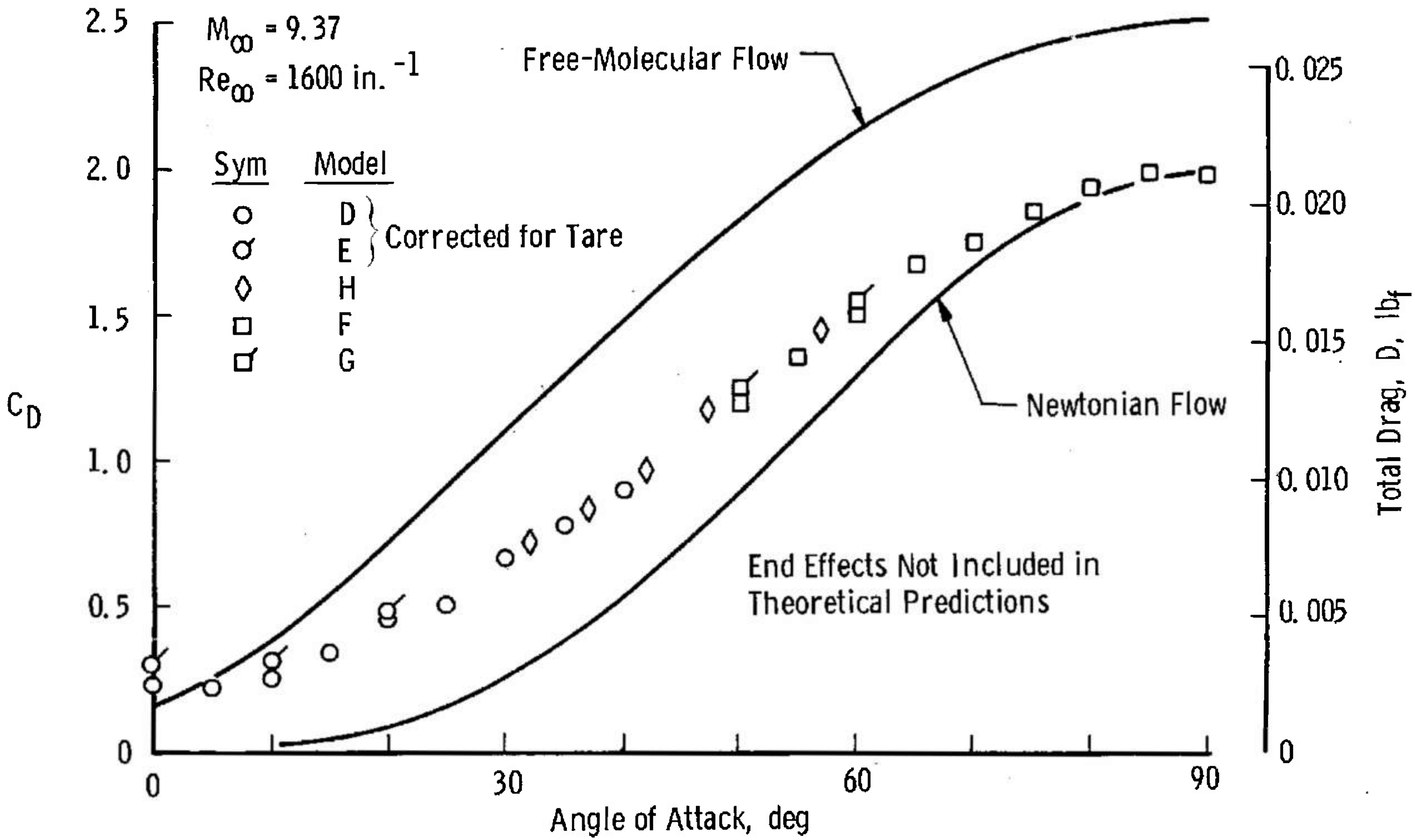

b. C_D as a Function of Angle of Attack

Fig. 6 Continued

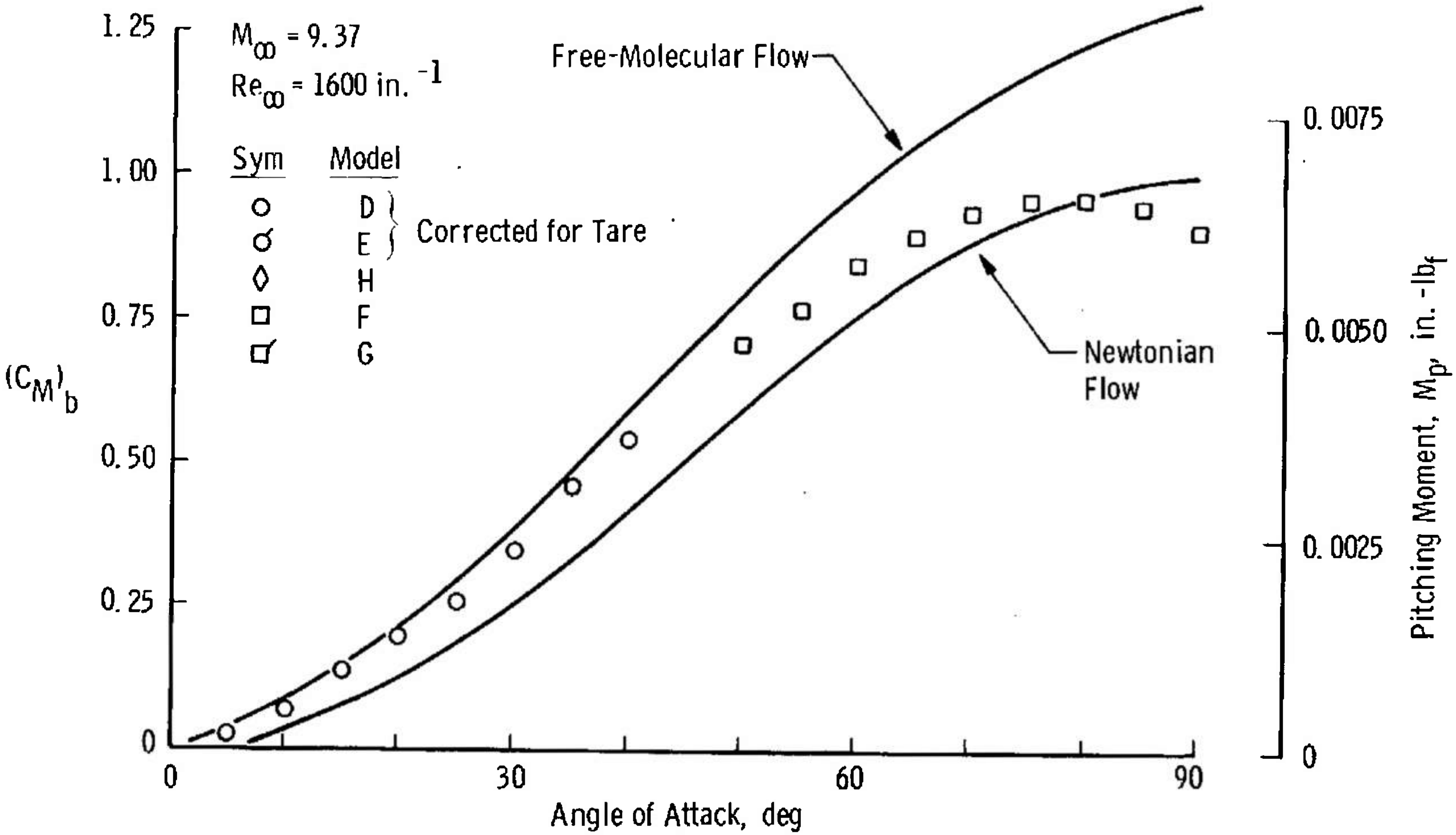

c. $(C_M)_b$ as a Function of Angle of Attack

Fig. 6 Continued

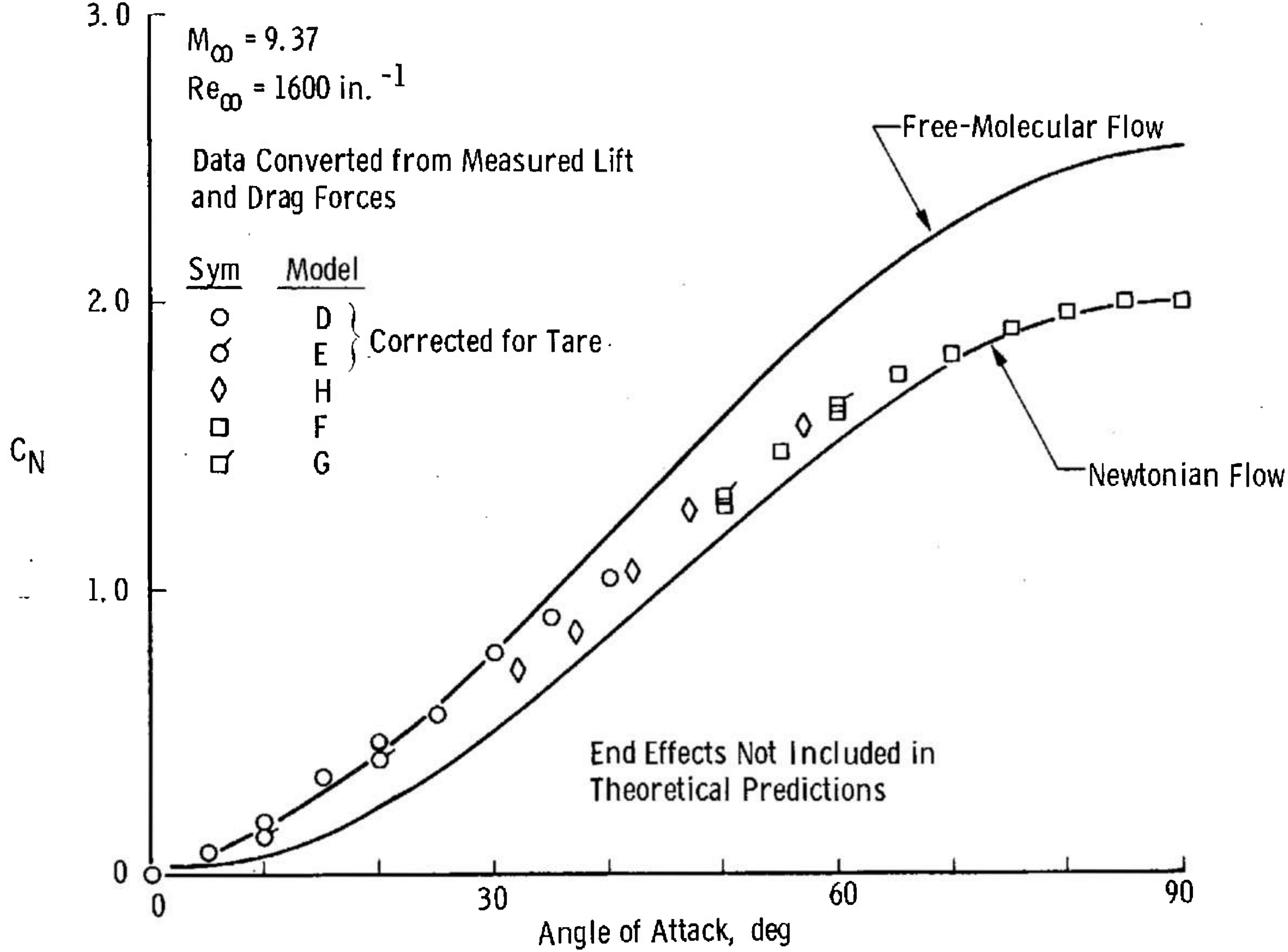

d. C_N as a Function of Angle of Attack

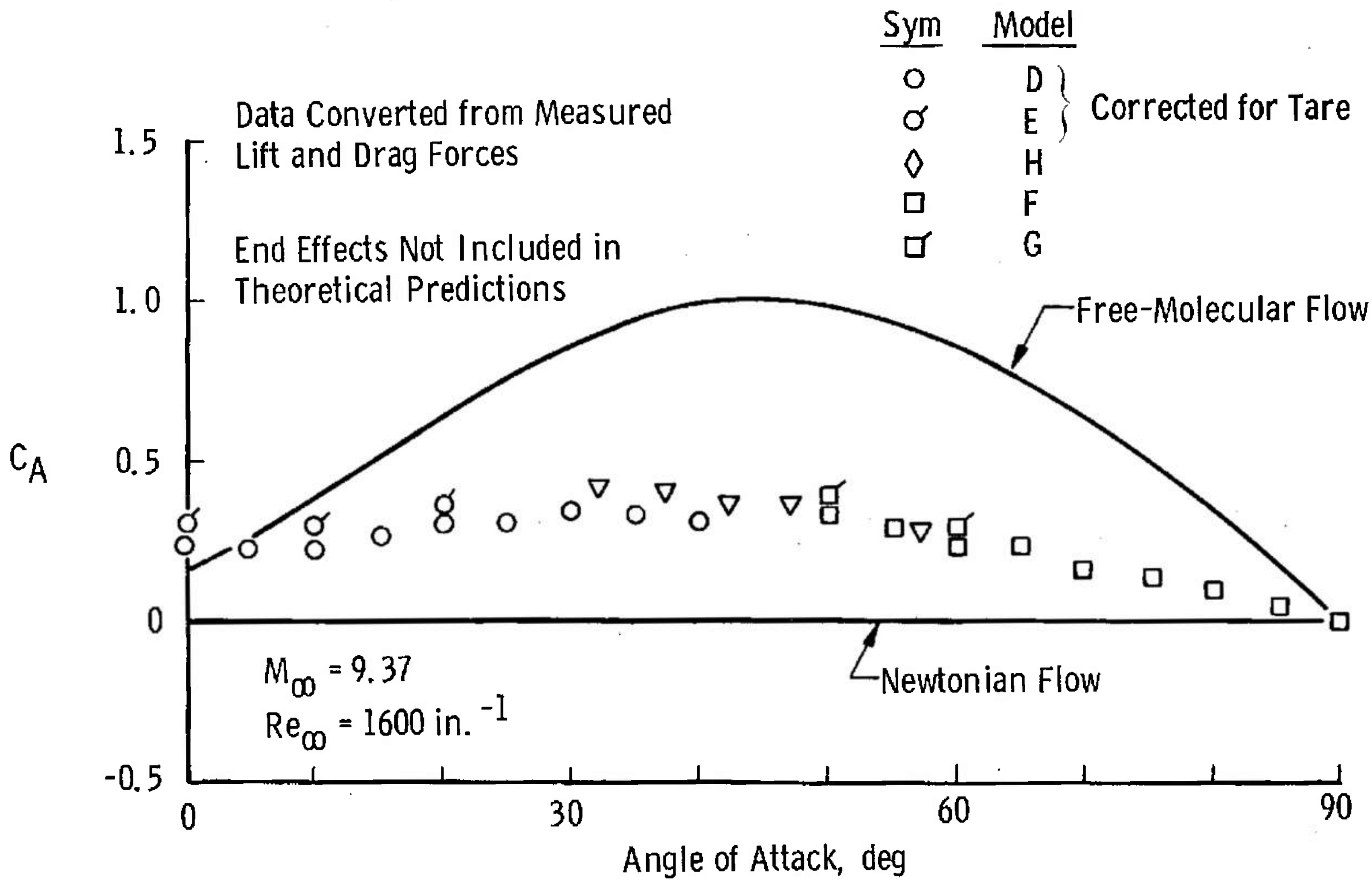

e. C_A as a Function of Angle of Attack

Fig. 6 Concluded

TABLE I
TABULATED TEST DATA

Fuel Capsule							
Model	α, deg	C_L	C_D	C_N	C_A	$(C_M)_{0.5\ell}$	$(C_M)_b$
A	0	-0.0015	2.311	-0.0015	2.311	0	0
↓	0	-0.0051	2.296	-0.0051	2.296	0	0
	2	-0.0246	2.328	-0.0567	2.327	-	-
	5	-0.0689	2.296	0.1315	2.293	-0.0124	0.0568
	8	-0.0988	2.328	0.2262	2.319	-	-
	10	-0.1375	2.336	0.2702	2.324	-0.0123	0.1234
	14	-0.1778	2.368	0.4004	2.341	-	-
	15	-	-	-	-	-0.0107	0.2105
	18.6	-0.1524	2.425	0.6290	2.347	-	-
	20	-	-	-	-	-0.004	0.3438
	24	-0.0902	2.490	0.9304	2.311	-	-
	25	-	-	-	-	-0.0154	0.4898
	29	0.0372	2.724	1.353	2.364	-	-
	30	-	-	-	-	-0.007	0.6818
	34.2	0.1487	2.910	1.759	2.323	-	-
	35	-	-	-	-	0.0292	0.9211
	39	0.2800	3.144	2.196	2.267	-	-
B	39.3	0.2176	3.136	2.152	2.291	-	-
↓	40	-	-	-	-	0.0642	1.136
	44.3	0.3419	3.339	2.575	2.153	-	-
	45	-	-	-	-	0.0940	1.379
	49.3	0.4825	3.500	2.966	1.919	-	-
	50	-	-	-	-	0.1148	1.595
	54.3	0.6192	3.702	3.366	1.660	-	-
	55	-	-	-	-	0.1306	1.781
	59.3	0.7014	3.864	3.679	1.373	-	-
	60	-	-	-	-	0.1343	1.929

TABLE I (Continued)

Fuel Capsule							
Model	α, deg	C_L	C_D	C_N	C_A	$(C_M)_{0.5\ell}$	$(C_M)_b$
C	58	0.6283	3.735	3.500	1.446	-	-
↓	60	-	-	-	-	0.1212	1.863
	65	0.6838	3.912	3.834	1.034	0.0969	1.974
	70	0.6695	4.000	3.988	0.7390	0.0768	2.064
	75	0.5748	4.131	4.139	0.5140	0.0639	2.129
	80	0.3975	4.220	4.225	0.3413	0.0402	2.158
	85	0.2446	4.292	4.297	0.1304	0.0072	2.156
	90	0.0235	4.325	4.325	-0.0235	-	2.131
A	-2	0.0229	2.336	-0.0586	2.335	-	-
↓	-5	0.0700	2.304	-0.1311	2.301	-	-
	-8	0.1003	2.320	-0.2236	2.311	-	-
	-10	0.1140	2.320	-0.2906	2.305	-	-
	-17	0.1538	2.344	-0.5382	2.287	-	-
	-21	0.1251	2.409	-0.7465	2.294	-	-
	-31.8	-0.0794	2.813	-1.550	2.349	-	-
B	-40.7	-0.2582	3.147	-2.250	2.216	-	-
↓	-45.7	-0.4000	3.371	-2.694	2.066	-	-
	-50.7	-0.5238	3.533	-3.067	1.830	-	-
	-60.7	-0.7194	3.799	-3.666	1.229	-	-
C	-62.5	-0.6780	3.799	-3.683	1.153	-	-
↓	-70	-0.6780	3.990	-3.981	0.7276	-	-
	-75	-0.5762	4.131	-4.139	0.5126	-	-
	-80	-0.3988	4.268	-4.272	0.3484	-	-
	-90	0.0125	4.300	-4.300	0.0125	-	-

TABLE I (Concluded)

Solar Panel							
Model	α, deg	C_L	C_D	C_N	C_A	$(C_M)_{0.5\ell}$	$(C_M)_b$
D*	0	0.0012	0.227	0.0012	0.227	-	0
↓	5	0.0628	0.222	0.0820	0.216	-	0.0234
	10	0.1469	0.248	0.1878	0.219	-	0.0684
	15	0.260	0.335	0.3378	0.257	-	0.1328
	20	0.327	0.449	0.4609	0.310	-	0.1981
	25	0.385	0.508	0.5636	0.297	-	0.2557
	30	0.479	0.672	0.7508	0.342	-	0.3483
	35	0.542	0.776	0.8891	0.325	-	0.4599
	40	0.588	0.903	1.0310	0.314	-	0.5388
E*	0	0.0117	0.297	0.0117	0.297	-	-
↓	10	0.098	0.313	0.1509	0.291	-	-
	20	0.256	0.476	0.4034	0.359	-	-
F	50	0.581	1.189	1.284	0.319	-	0.705
↓	55	0.599	1.360	1.458	0.289	-	0.766
	60	0.591	1.503	1.598	0.240	-	0.843
	65	0.527	1.678	1.744	0.231	-	0.895
	70	0.462	1.747	1.800	0.164	-	0.937
	75	0.366	1.862	1.894	0.128	-	0.959
	80	0.239	1.941	1.954	0.102	-	0.960
	85	0.127	1.987	1.991	0.046	-	0.942
	90	0.0064	1.982	1.982	-0.0064	-	0.906
G	50	0.545	1.252	1.309	0.387	-	-
↓	60	0.569	1.549	1.626	0.282	-	-
H	32	0.383	0.724	0.7085	0.411	-	-
↓	37	0.462	0.839	0.8739	0.392	-	-
	42	0.539	0.973	1.052	0.362	-	-
	47	0.597	1.180	1.270	0.368	-	-
	57	0.609	1.448	1.546	0.278	-	-

*Corrected for tare

APPENDIX I
TUNNEL L

TUNNEL DESCRIPTION

Tunnel L, shown in Fig. I-1, is a low density, hypersonic, continuous-type, arc-heated, ejector-pumped facility, normally using nitrogen or argon as the test gas and consisting of the following major components, in streamwise order:

1. Continuous, water-cooled, d-c arc heater, Thermal Dynamic F-40 or U-50, both modified slightly, with a 40-kw selenium rectifier power supply. Gas is injected without swirl in the F-40 arc heater and with or without swirl in the U-50 unit. Unless otherwise noted, all testing is done without use of swirling gas injection.
2. Cylindrical, water-cooled settling section of variable size, but normally of 3-in. diameter and 6- to 10-in. length
3. Axisymmetric, aerodynamic nozzle, variable sizes with 0.10- to 1.20-in.-diam throats and 2.0- to 8.2-in.-diam exits. Three contoured nozzles having no flow gradients in the test section are currently available, in addition to older conical nozzles. Table I-1 gives the major characteristics of the contoured nozzles.
4. Cylindrical test section tank of 48-in. diameter surrounding the test section and containing instrumentation, cooling water connections, and probe carrier
5. Axisymmetric diffuser with interchangeable designs for varying test conditions, convergent entrance, constant-area throat, divergent exit sections, and water-cooled entrance
6. Water-cooled heat exchanger
7. Isolation valve
8. Air ejector of two stages
9. Connection to the VKF evacuated, 200,000-cu-ft, spherical vacuum reservoir and its pumping system.

All critical components of the tunnel and related systems are protected by back-side water cooling. The two-stage ejector system is driven by air instead of steam because of the ready availability of high pressure air at the tunnel site. Although the working gas is normally nitrogen or argon, other gases may be used. Typical ranges of operation with heated flow are given in Table I-2, and unheated-flow operational ranges are given in Table I-3. The first published description of this tunnel appeared in Ref. I-1.

TUNNEL INSTRUMENTATION AND CALIBRATION

Gas flow rate to the arc heater is measured through use of calibrated sonic-flow orifices, and reservoir pressure is measured with a Consolidated Electrodynamics Corporation Electromanometer®. Inaccuracy of these systems, on the basis of comparison with other means of measurement, and repeatability are estimated to be less than ±0.5 percent for both flow rate and reservoir pressure.

Total enthalpy at the nozzle throat is determined by use of a calorimeter which, on the basis of comparison of results and repeatability, appears accurate to within ±4 percent limits of error. This measurement is supplemented by a probe system which measures local total enthalpy and mass flux in the test section with an estimated error limit of ±2 percent for mass flux and ±5 percent for enthalpy.

Impact pressures are measured with variable reluctance, differential pressure transducers and water-cooled probes. Calibration of the transducers is accomplished by means of an oil-filled micromanometer and a McLeod gage. Inaccuracy in impact pressure measurement is believed not to exceed ±2 percent limits. Static pressures are measured by the same method but are not used for primary calibration purposes because of the very large corrections for viscous- and rarefied-flow phenomena.

The establishment of reservoir conditions, determination of impact pressures, and proof of inviscid, adiabatic core flow through the nozzles form part of the flow calibration. This information is used in a calculation which accounts for nonequilibrium expansion of the gas throughout the nozzle to yield the needed flow properties. References I-2 through I-7 contain information on various aspects of these measurements.

A three-component balance is used for measuring lift, drag, and pitching moment on aerodynamic bodies in Tunnel L. This is described in Ref. I-8.

REFERENCES

I-1. Potter, J. L., Kinslow, M., Arney, G. D., Jr., and Bailey, A. B. "Initial Results from a Low-Density Hypervelocity Wind Tunnel." Progress in Astronautics and Rocketry, Ed. by F. R. Riddell, Academic Press, New York, 1962, pp. 599-624.

I-2. Potter, J. L., Arney, G. D., Jr., Kinslow, M., and Carden, W. H. "Gasdynamic Diagnosis of High-Speed Flows Expanded from Plasma States." IEEE Transactions on Nuclear Science, Vol. NS-11, No. 1, January 1964, pp. 145-157.

I-3. Potter, J. L., Arney, George D., Jr., Carden, William H., and Kinslow, Max. "Irreversible Flow in Reservoir and Throat Sections of Wind Tunnels with Constricted-Arc Heaters." Proceedings of AGARD Fluid Dynamics Panel Specialists Meeting, Arc Heaters and MHD Accelerators for Aerodynamic Purposes." AGARDograph 84, September 1964, pp. 379-412.

I-4. Kinslow, Max and Miller, J. T. "The Nonequilibrium Expansion of a Diatomic Gas through a Convergent-Divergent Nozzle." AEDC-TR-65-103 (AD464533), June 1965.

I-5. Potter, J. Leith and Bailey, Allan B. "Pressures in the Stagnation Regions of Blunt Bodies in the Viscous-Layer to Merged-Layer Regimes of Rarefied Flow." AEDC-TDR-63-168 (AD416004), September 1963.

I-6. Potter, J. Leith, Kinslow, Max, and Boylan, David E. "Influence of the Orifice on Measured Pressures in Rarefied Flow." Presented at the Fourth International Symposium on Rarefied Gas Dynamics, July 14-17, 1964.

I-7. Carden, William H. "Experimental Heat Transfer to Hemispheres in Nonequilibrium Dissociated Hypersonic Flow with Surface Catalysis and Second-Order Effects." AEDC-TR-65-127 (AD466165), July 1965. (Also Preprint No. 66-3 for the AIAA Third Aerospace Sciences Meeting, New York, January 24-27, 1966.

I-8. Arney, G. D. and Harter, W. T. "A Low-Load Three Component Force Balance for Measurements in a Low-Density Wind Tunnel." IEEE Transactions on Aerospace, Vol. AS-3, No. 1, February 1965, pp. 3-8.

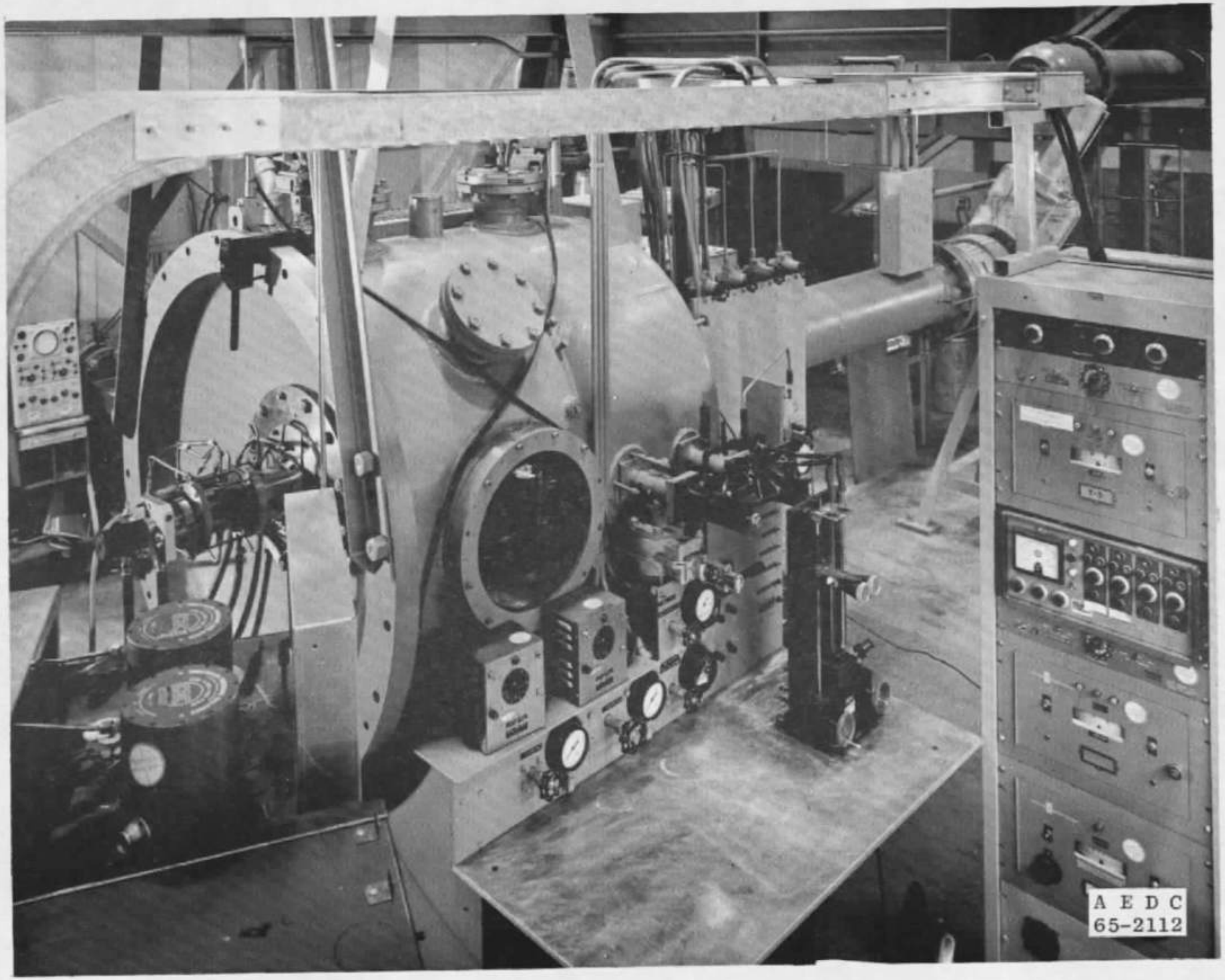

Fig. 1-1 Tunnel L

TABLE I-1
MAJOR CHARACTERISTICS OF TUNNEL L CONTOURED NOZZLES

	Lower Reynolds No.	Higher Reynolds No.	Cold Flow
Total Pressure, psia	18.0	30.0	0.235
Total Temperature, °R	5400	4500	530
Mass Flow Rate, lb_m/hr	7.76	14.2	22
Throat Diameter, in.	0.1481	0.1469	1.2226
Exit Diameter, in.	8.160	4.814	5.494
Test Section Core Diameter, in.	1.5	2.0	3.2
Test Section M_∞	10.15	9.3	4.05
Test Section Unit Reynolds No., $in.^{-1}$	388	1200	1760

TABLE I-2
TUNNEL L OPERATING CONDITIONS WITH ARC HEATER

	Nitrogen	Argon
Total Pressure, psia	7.0 to 30.0	0.5 to 6.4
Total Enthalpy, Btu/lb_m	740 to 2130	280 to 960
Total Temperature, °R	2300 to 7200	2300 to 7700
Mach Number	4.8 to 10.8	3.7 to 16.1
Unit Reynolds Number, Free Stream, $in.^{-1}$	300 to 3500	270 to 4700
Unit Reynolds Number behind Normal Shock, $in.^{-1}$	35 to 1140	14 to 1080
Mean Free-Path, Free-Stream, Static Billiard-Ball Gas Model, in.	0.002 to 0.058	0.002 to 0.05
Uniform Flow Core Diameter at Test Section, in.	0.2 to 2.0	0.5 to 1.5

TABLE I-3
TUNNEL L OPERATING CONDITIONS WITHOUT ARC HEATER

	Nitrogen	Argon
Total Pressure, psia	0.06 to 2.7	0.08 to 3.0
Total Enthalpy, Btu/lb_m	140	70
Total Temperature, °R	530	530
Mach Number	3.8 to 5.8	4.0 to 8.0
Unit Reynolds Number Free Stream, $in.^{-1}$	620 to 15,000	1600 to 50,000
Unit Reynolds Number behind Normal Shock, $in.^{-1}$	190 to 3500	264 to 3800
Mean Free-Path, Free-Stream, Static Billiard-Ball Gas Model, in.	0.0005 to 0.012	0.0001 to 0.006
Uniform Flow Core Diameter at Test Section, in.	0.8 to 3.2	0.5 to 1.0

UNCLASSIFIED
Security Classification

DOCUMENT CONTROL DATA - R&D

(Security classification of title, body of abstract and indexing annotation must be entered when the overall report is classified)

1. ORIGINATING ACTIVITY (Corporate author) Arnold Engineering Development Center ARO, Inc., Operating Contractor Arnold Air Force Station, Tennessee	2a. REPORT SECURITY CLASSIFICATION UNCLASSIFIED 2b. GROUP N/A

3. REPORT TITLE
AERODYNAMIC FORCES ON THE SNAP-19 FUEL CAPSULE AND NIMBUS B SOLAR PANEL AT A SIMULATED HIGH ALTITUDE

4. DESCRIPTIVE NOTES (Type of report and inclusive dates)
N/A

5. AUTHOR(S) (Last name, first name, initial)
Boylan, David E., ARO, Inc.

This document has been approved for public release its distribution is unlimited. Per ... letter ...

6. REPORT DATE	7a. TOTAL NO. OF PAGES	7b. NO. OF REFS
September 1966	44	6

8a. CONTRACT OR GRANT NO. AF 40(600)-1200 b. AEC SNAP 19 Program c. AEC Activity Nr. 04-60-50-01.1 d.	9a. ORIGINATOR'S REPORT NUMBER(S) AEDC-TR-66-162 9b. OTHER REPORT NO(S) (Any other numbers that may be assigned this report) N/A

10. AVAILABILITY/LIMITATION NOTICES
~~Qualified users may obtain copies of this report from DDC. Release to foreign governments or foreign nationals may be made only with prior approval of AEC, Albuquerque, N.M.~~

11. SUPPLEMENTARY NOTES	12. SPONSORING MILITARY ACTIVITY
N/A	Atomic Energy Commission Albuquerque, N.M.

13. ABSTRACT

Aerodynamic forces on a SNAP-19 fuel capsule and Nimbus B solar panel model were determined over an angle-of-attack range from 0 to 90 deg at a simulated high altitude under hypersonic, cold-wall conditions. Very large viscous-induced effects on aerodynamic drag, lift, and pitching moment were observed. The configurations were unstable about their mid-chord positions except near zero lift. Comparisons are made with inviscid (Newtonian) and free-molecular flow predictions. Altitude simulated for the full-scale configurations was approximately 260,000 ft for the fuel capsule and 300,000 ft for the solar panel.

DD FORM 1 JAN 64 1473

UNCLASSIFIED
Security Classification

UNCLASSIFIED
Security Classification

14. KEY WORDS	LINK A		LINK B		LINK C	
	ROLE	WT	ROLE	WT	ROLE	WT
aerodynamic forces SNAP-19 nuclear power generator Nimbus B solar panels 2. Nimbus B solar panels. ~~3. Nimbus~~ 4. Nuclear reactors -- Snap 19. 5. Nuclear fuel						

15-14

INSTRUCTIONS

1. ORIGINATING ACTIVITY: Enter the name and address of the contractor, subcontractor, grantee, Department of Defense activity or other organization (*corporate author*) issuing the report.

2*a*. REPORT SECURITY CLASSIFICATION: Enter the overall security classification of the report. Indicate whether "Restricted Data" is included. Marking is to be in accordance with appropriate security regulations.

2*b*. GROUP: Automatic downgrading is specified in DoD Directive 5200.10 and Armed Forces Industrial Manual. Enter the group number. Also, when applicable, show that optional markings have been used for Group 3 and Group 4 as authorized.

3. REPORT TITLE: Enter the complete report title in all capital letters. Titles in all cases should be unclassified. If a meaningful title cannot be selected without classification, show title classification in all capitals in parenthesis immediately following the title.

4. DESCRIPTIVE NOTES: If appropriate, enter the type of report, e.g., interim, progress, summary, annual, or final. Give the inclusive dates when a specific reporting period is covered.

5. AUTHOR(S): Enter the name(s) of author(s) as shown on or in the report. Enter last name, first name, middle initial. If military, show rank and branch of service. The name of the principal author is an absolute minimum requirement.

6. REPORT DATE: Enter the date of the report as day, month, year; or month, year. If more than one date appears on the report, use date of publication.

7*a*. TOTAL NUMBER OF PAGES: The total page count should follow normal pagination procedures, i.e., enter the number of pages containing information.

7*b*. NUMBER OF REFERENCES: Enter the total number of references cited in the report.

8*a*. CONTRACT OR GRANT NUMBER: If appropriate, enter the applicable number of the contract or grant under which the report was written.

8*b*, 8*c*, & 8*d*. PROJECT NUMBER: Enter the appropriate military department identification, such as project number, subproject number, system numbers, task number, etc.

9*a*. ORIGINATOR'S REPORT NUMBER(S): Enter the official report number by which the document will be identified and controlled by the originating activity. This number must be unique to this report.

9*b*. OTHER REPORT NUMBER(S): If the report has been assigned any other report numbers (*either by the originator or by the sponsor*), also enter this number(s).

10. AVAILABILITY/LIMITATION NOTICES: Enter any limitations on further dissemination of the report, other than those imposed by security classification, using standard statements such as:

(1) "Qualified requesters may obtain copies of this report from DDC."

(2) "Foreign announcement and dissemination of this report by DDC is not authorized."

(3) "U. S. Government agencies may obtain copies of this report directly from DDC. Other qualified DDC users shall request through ______________."

(4) "U. S. military agencies may obtain copies of this report directly from DDC. Other qualified users shall request through ______________."

(5) "All distribution of this report is controlled. Qualified DDC users shall request through ______________."

If the report has been furnished to the Office of Technical Services, Department of Commerce, for sale to the public, indicate this fact and enter the price, if known.

11. SUPPLEMENTARY NOTES: Use for additional explanatory notes.

12. SPONSORING MILITARY ACTIVITY: Enter the name of the departmental project office or laboratory sponsoring (*paying for*) the research and development. Include address.

13. ABSTRACT: Enter an abstract giving a brief and factual summary of the document indicative of the report, even though it may also appear elsewhere in the body of the technical report. If additional space is required, a continuation sheet shall be attached.

It is highly desirable that the abstract of classified reports be unclassified. Each paragraph of the abstract shall end with an indication of the military security classification of the information in the paragraph, represented as (*TS*), (*S*), (*C*), or (*U*).

There is no limitation on the length of the abstract. However, the suggested length is from 150 to 225 words.

14. KEY WORDS: Key words are technically meaningful terms or short phrases that characterize a report and may be used as index entries for cataloging the report. Key words must be selected so that no security classification is required. Identifiers, such as equipment model designation, trade name, military project code name, geographic location, may be used as key words but will be followed by an indication of technical context. The assignment of links, rules, and weights is optional.

UNCLASSIFIED
Security Classification